1976-03

Charge and current distributions on, and input impedance of moderately fat transmitting crossed-monopole antennas.

McDowell, Elmer Jay

Monterey, California. Naval Postgraduate School

CHARGE AND CURRENT DISTRIBUTIONS ON, AND INPUT IMPEDANCE OF MODERATELY FAT TRANSMITTING CROSSED-MONOPOLE ANTENNAS

Elmer Jay McDowell

Report Number NPS52Zn76031

NAVAL POSTGRADUATE SCHOOL
Monterey, California

THESIS

CHARGE AND CURRENT DISTRIBUTIONS ON,
AND INPUT IMPEDANCE OF
MODERATELY FAT TRANSMITTING
CROSSED-MONOPOLE ANTENNAS

Elmer Jay McDowell

March 1976

Thesis Advisor: R. W. Burton

Prepared for: Air Force Weapons Laboratory/PRP
Kirtland AFB
New Mexico 87117

REPORT DOCUMENTATION PAGE

READ INSTRUCTIONS BEFORE COMPLETING FORM

1. REPORT NUMBER: NPS52Zn76031
2. GOVT ACCESSION NO.:
3. RECIPIENT'S CATALOG NUMBER:

4. TITLE (and Subtitle): CHARGE AND CURRENT DISTRIBUTIONS ON, AND INPUT IMPEDANCE OF MODERATELY FAT TRANSMITTING CROSSED-MONOPOLE ANTENNAS

5. TYPE OF REPORT & PERIOD COVERED: Final Report 1 June 75 - 1 March 76

6. PERFORMING ORG. REPORT NUMBER:

7. AUTHOR(s): Elmer J. McDowell in conjunction with Robert W. Burton

8. CONTRACT OR GRANT NUMBER(s):

9. PERFORMING ORGANIZATION NAME AND ADDRESS: Naval Postgraduate School Monterey, California 93940

10. PROGRAM ELEMENT, PROJECT, TASK AREA & WORK UNIT NUMBERS:

11. CONTROLLING OFFICE NAME AND ADDRESS: Air Force Weapons Laboratory/PRP Kirtland AFB New Mexico 87117

12. REPORT DATE: March 1976

13. NUMBER OF PAGES: 118

14. MONITORING AGENCY NAME & ADDRESS (if different from Controlling Office):

15. SECURITY CLASS. (of this report): Unclassified

15a. DECLASSIFICATION/DOWNGRADING SCHEDULE:

16. DISTRIBUTION STATEMENT (of this Report)

Approved for public release, distribution unlimited.

17. DISTRIBUTION STATEMENT (of the abstract entered in Block 20, if different from Report)

18. SUPPLEMENTARY NOTES

19. KEY WORDS (Continue on reverse side if necessary and identify by block number)

Surface Charge and Current Distribution
Crossed-Monopole
Junction Charge

20. ABSTRACT (Continue on reverse side if necessary and identify by block number)

Charge and current distributions in the vicinity of the cross junction for several configurations of electrically long, moderately fat crossed-monopole transmitting antennas over a ground plane were measured and compared with the equivalent monopole. The input impedance of these configurations at the ground plane/antenna interface was also experimentally determined. Junction conditions such that there would be a maximum current/minimum

(20. ABSTRACT Continued)

charge and minimum current/maximum charge on the vertical monopole were examined. The effect on the input impedance and current/charge distribution of adding resonant and antiresonant horizontal cross members to the junction was investigated and displayed. For purposes of physical understanding, a zero-order explanation was given in terms of the multiple resonances present on the crossed-monopole as compared with the reference monopole.

NAVAL POSTGRADUATE SCHOOL
Monterey, California

Rear Admiral Isham W. Linder
Superintendent

Jack R. Borsting
Provost

This thesis was prepared in conjunction with research supported in part by AFWL/PRP under Project numbers 75-002 and 76-211.

Released as a
technical report by:

Charge and Current Distributions on, and Input Impedance of Moderately Fat Transmitting Crossed-Monopole Antennas

by

Elmer Jay McDowell
Lieutenant Commander, United States Navy
B.S.E.E. Purdue University, 1966

Submitted in partial fulfilment of the
requirements for the degree of

MASTER OF SCIENCE IN ELECTRICAL ENGINEERING

from the
NAVAL POSTGRADUATE SCHOOL
March 1976

ABSTRACT

Charge and current distributions in the vicinity of the cross junction for several configurations of electrically long, moderately fat crossed-monopole transmitting antennas over a ground plane were measured and compared with the equivalent monopole. The input impedance of these configurations at the ground plane/antenna interface was also experimentally determined. Junction conditions such that there would be a maximum current/minimum charge and minimum current/maximum charge on the vertical monopole were examined. The effect on the input impedance and current/charge distribution of adding resonant and antiresonant horizontal cross members to the junction was investigated and displayed. For purposes of physical understanding, a zero-order explanation was given in terms of the multiple resonances present on the crossed-monopole as compared with the reference monopole.

TABLE OF CONTENTS

ACKNOWLEDGEMENT

This thesis is a summary of my research efforts over the past six months. Any success which I may have had in these efforts is directly attributable to the patient guidance provided by Associate Professor R. W. Burton of the Naval Postgraduate School. I also received invaluable assistance from my daughter Heather whose patience as a data recorder often surpassed my own. For this guidance and assistance, and for the moral support provided by my wife Rose-Marie I reserve my deepest gratitude.

I. INTRODUCTION

A. BACKGROUND

The distributions of current and charge that are induced on conducting surfaces of various configurations by external electromagnetic fields have been experimentally and analytically investigated with varying degrees of intensity over the past several decades. Impetus has been given to these investigations by the revelation of the Electromagnetic Pulse (EMP) associated with a nuclear detonation and its apparent electromagnetic effects on missiles, aircraft, shielded transmission lines and other metal-clad structures.

Early experimental work in this area focused on quantifying the charge and current distributions on electrically thin cylindrical dipoles. The early theory dealt with straight perfect conductors of zero radius over a lossless infinite ground plane. The characteristics of straight cylindrical antennas are now well known [King 1946]. Later theory expanded on these ideal conditions, but remained centered on primitive shapes due to the complexity of the problem. A growing body of experimental data on more complex configurations has provided the basis for some

understanding of the effects of EMP.

The crossed-dipole receiving antenna is commonly used as a model for the prediction of EMP effects on aircraft [Taylor 1969; Taylor et al. 1970; Butler 1972; Chao and Strait 1972]. Experimental measurements on thin crossed antennas in a plane-wave electromagnetic field provided the basis for physical insight into this phenomena [Burton 1974].

The experimental [Burton and King 1975] and analytical [King and Wu 1975] investigations of the crossed-dipole scattering antenna have shown that resonances with large amplitude standing waves of current and charge can occur in such a way that all combinations of charge and current maxima and minima can occur at the junction of the cross at various excitation frequencies. The results for scattering crossed-dipole antennas have been extended by examining the impedance of various crossed-dipole antennas in the transmitting mode over a broad range of microwave frequencies [Spencer 1975].

B. THESIS

With sufficient knowledge of the resonances of, and charge and current distributions on, a crossed-monopole structure it could begin to be analyzed as an antenna for radiating or receiving electromagnetic energy at specific frequencies. In the same way that the crossed-dipole receiving antenna was used as a model for the prediction of EMP effects on aircraft it could be used to enhance the understanding of the resonances and charge and current distributions present on aircraft or ship structures excited in the transmitting mode.

C. THESIS OBJECTIVE

The major objectives of this work were to experimentally determine the charge and current distributions in the vicinity of the junction on several configurations of crossed-monopole transmitting antennas, to investigate the input impedance of these configurations at the ground plane/antenna interface, and to provide physical insight into the phenomena through a consideration of the multiple resonances present on the members (arms).

The secondary objectives were to improve the machining techniques for construction of charge and current distribution measurement devices and to continue development

of instrumentation for convenient measurement and data manipulation at the Naval Postgraduate School.

II. THEORY

A. MONOPOLES

The classical ideal monopole antenna located over ideal ground is assumed to have charge and current sinusoidally distributed over its length when driven by a sinusoidal source impressing a rotationally symmetric electric field across an infinitely thin base separation. End point boundary conditions (zero current/maximum charge) and the electrical length of the monopole determine the phase of these distributions. Variations from the ideal take the form of perturbations of the sinusoidal distribution (a result of the non-zero radii of real conductors), non-zero current at the end (also a result of non-zero radii permitting current to flow on the end), and distortion of the impressed voltage (a result of the impracticality of a slice generator).

A monopole which permits the current to distribute itself an odd number of quarter-wavelengths over its length will have an assumed zero current at the end and thus a current maximum at the feed point. The charge in such a monopole will accumulate at the end and deplete at the feed point. Figure 1 (a) illustrates these ideal distributions

for the situation where the monopole is three quarter wavelengths long (n=3 in: Height = n $\lambda/4$). For this configuration the current is in time phase with the voltage at the feed point and the impedance is real and minimum. Such an antenna is said to be resonant.

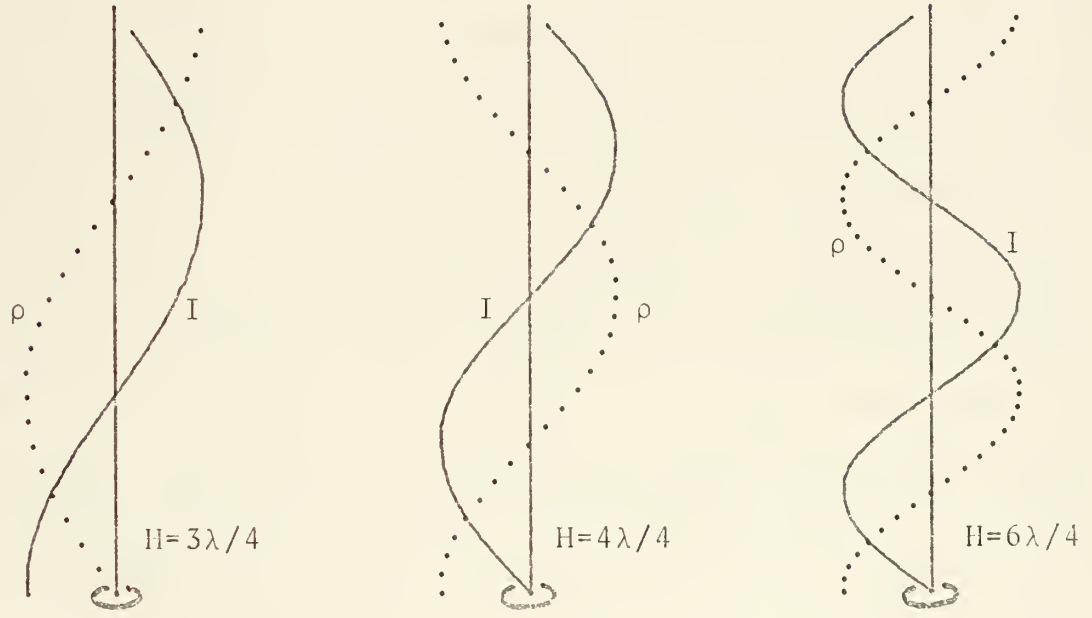

Figure 1. -
Assumed Monopole Charge and Current Distributions

A monopole electrically an even number of quarter wavelengths in length (n even in: Height = n $\lambda/4$) with the same end boundary conditions and assumed ideal distributions will exhibit a current minimum and charge maximum at the feed point. In this case the charge and current remain in

time phase at the feed point; however, the impedance is a real maximum and the antenna is said to be antiresonant [King 1956]. Figure 1 (b) and (c) illustrates these distributions for the cases of n=4 and n=6 respectively.

Monopoles whose electrical length dictates neither resonance nor antiresonance present a complex impedance at the antenna/ground plane interface. The nature of the complex impedance depends on whether the monopole is shorter or longer than that required for resonance or antiresonance. An electrical length slightly shorter than the resonant length or slightly longer than the antiresonant length results in a capacitive input. On the other hand, an electrical length slightly longer than the resonant length or slightly shorter than the antiresonant length results in an inductive impedance at the antenna/feed interface [King 1956, p. 159].

B. CROSSED-MONOPOLES

When the monopole is crossed by a perpendicular element creating a junction, analysis is somewhat more complicated by the effects taking place at the junction. Intuitively it would appear that currents on each of the elements, in the vicinity of the junction, would obey Kirchoff's Current Law and that the surface charge on each of the elements would

approach a common value as the junction was approached. It has been shown that this is the case for crossed-dipoles constructed of electrically thin cylinders [Burton and King 1975, King and Wu 1975].

For consideration of the impedance seen at the feed point, the simplest view of the crossed-monopole is as a loaded vertical monopole. The effect of the loading at the junction is to provide additional conductors on which current can flow and charge can accumulate. This situation can be thought of as creating a capacitance effect between the loading elements and the image plane effectively adding capacitance in parallel with the antenna. Addition of parallel capacitance causes antiresonance to occur at shorter monopole heights [King 1956, p. 198], thus a given height antenna appears slightly longer. While this view is adequate for an impression of the effect on the input impedance, a more comprehensive view may be developed through consideration of the resonances of the arms as individual elements excited by the junction.

With the arm elements connected perpendicular to the monopole there is no inductive coupling between the monopole and the arm. The electric (E) field emanating from the monopole is oriented radially (axially with the arms) so as to induce opposing currents in opposite arms. The magnitude

of these induced currents and thus the magnitude of the charge and current distributions in the arms is proportional to the strength of the E field (which is directly related to the surface charge in the proposed junction region).

Physical insight into the induced charge and current distributions in the perpendicular arms of the crossed-monopole can be gained by consideration of the forces acting between free charge in the arms and the surface charge density in the standing-wave pattern of charge on the vertical element.

Figure 2 (a) shows the zero-order approximation of charge on the vertical member with the junction imposed at a point of charge minimum. The junction is located within the charge standing-wave pattern in such a way that from any point on the horizontal arm the equidistant charge in the charge standing-wave pattern above and below the junction on the vertical member is 180 degrees out of phase. These equidistant charge densities of equal magnitude and opposite sign on the vertical member contribute mutually canceling axial forces on the free charge at all points along the horizontal arms. If physical symmetry of the vertical member with the junction did not exist, the axial force in the arms from some charge, remotely located from the junction, would not be canceled by the effect of oppositely

polarized, equidistant charge. Since these uncancelled forces would result from charge relatively distant, they would be quite small. A more realistic (higher order) approximation of charge distribution on the vertical member would show a non-zero minimum of charge at the proposed junction. Forces resulting from this charge minimum, although nearly axially directed and uncanceled, would also be relatively small.

In Figure 2 (b) the charge distribution on the vertical member is again represented by a zero-order approximation. The junction is now located at a point of charge maximum in the standing-wave pattern. In this case the concentration of charge in the immediate junction area exerts nearly axial force on free charge in the arm. Canceling forces originating from charges removed from the junction by one quarter-wavelength have negligibly small axial components. A large axial force is therefore exerted on the charges distributed along the arm in this case.

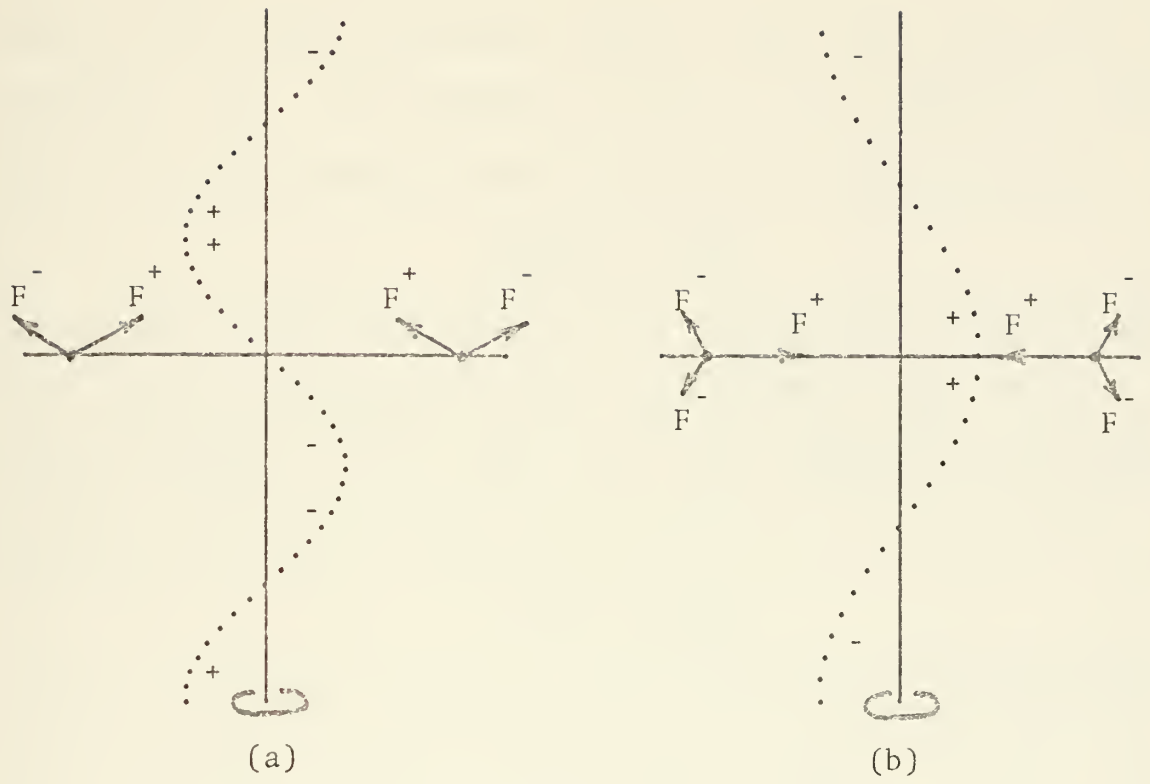

Figure 2. -
Illustration of Forces Acting on Charges
in Horizontal Elements

Positioning the arms at a point of maximum charge on the monopole generates large axial forces acting on charge in the arms. This induces charge and current distributions on the arms of relatively large magnitude. Conversely, when the arms are positioned at a point of minimum charge the axial forces on charge in the arms are small and the charge and current distribution amplitudes generated on the arms are also small.

Current distributions induced in equal length opposite arms by the forces described above are odd functions of distance frcm the junction. That is, for x directed along the horizontal elements with the origin at the junction,

$$I(-x) = -I(x).$$

The induced charge distribution in these arms, forced by the end boundary condition and the requirement for charge in each element to be equal at the junction, is an even function of distance from the junction:

$$\rho(-x) = \rho(x)$$

These conditions describe charge and current distributions on an antisemetrically driven dipole. Figure 3 (a) and (b) illustrates these distributions on horizontal dipoles of half length one-half-wavelength and one-quarter-wavelength respectively.

When Figure 3 (a) is superimposed on Figure 1 (b) a condition is seen to exist where the system is totally antiresonant. All elements and combinations of elements are antirescnant lengths. All boundary conditions are satisfied. Charge is maximum and current minimum at the junction for each element. No other combination of Figures 3 (a) and (b) with Figures 1 (b) and (c) produces a condition where all elements and combinations of elements are either resonant or antiresonant. Combinations of the

elements in these figures (as later defined) form the basis for this investigation.

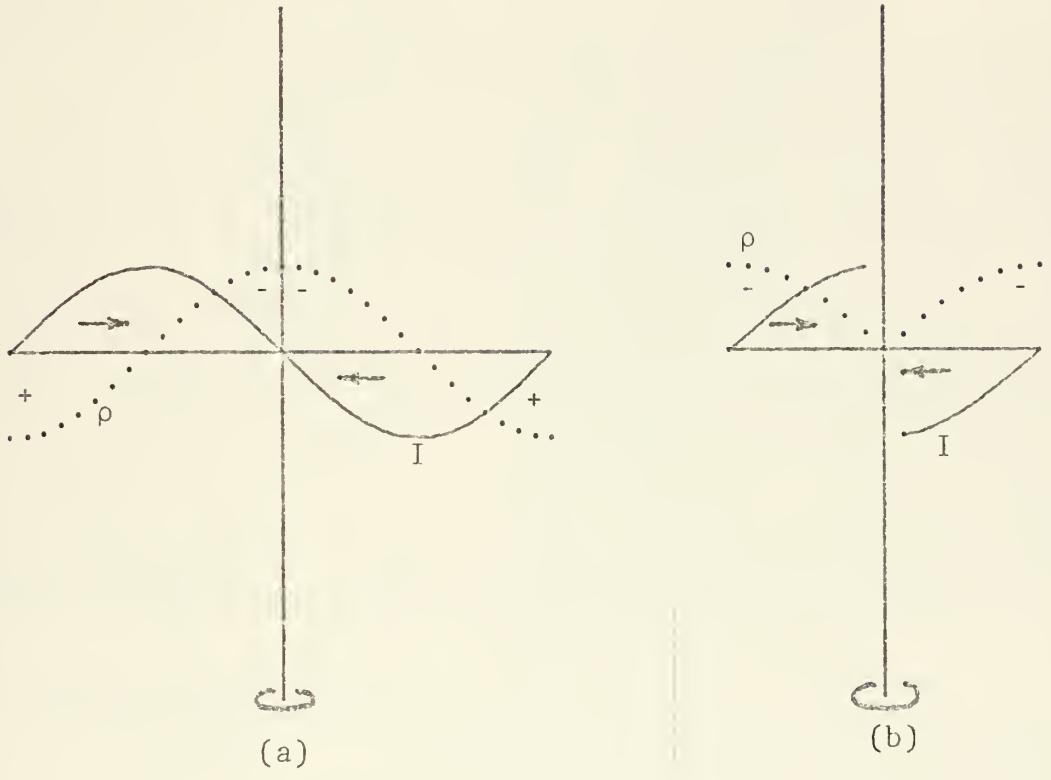

Figure 3. -
Assumed Charge and Current Distributions on Half and Quarter-Wavelength Horizontal Elements.

III. EXPERIMENTAL SET-UP

A. IMAGE PLANE

Experimental measurements reported herein were taken with the antenna above a 10 meter square aluminum surface serving as an image (ground) plane for the antenna. This aluminum surface formed the roof for a room in which the antenna feed system and measurement equipment were located, and from which the measurement position could be controlled. The image plane structure with a CASE 4 (later defined) crossed-monopole antenna installed is shown in Figure 4.

B. ANTENNA FEED SYSTEM

In addition to providing a method of coupling electromagnetic energy to the antenna, the antenna feed system provided support for the antenna, a method of mounting the antenna above the ground plane, and access to the antenna through the interior of the center conductor. The feed system also provided a reference impedance for determination of antenna input impedance.

Six inch and 2.5 inch brass tubing, placed concentrically formed the coaxial feed line. One end was shorted by a brass end plate to which the tubing was soldered. The other end was closed by a 3/8 inch thick

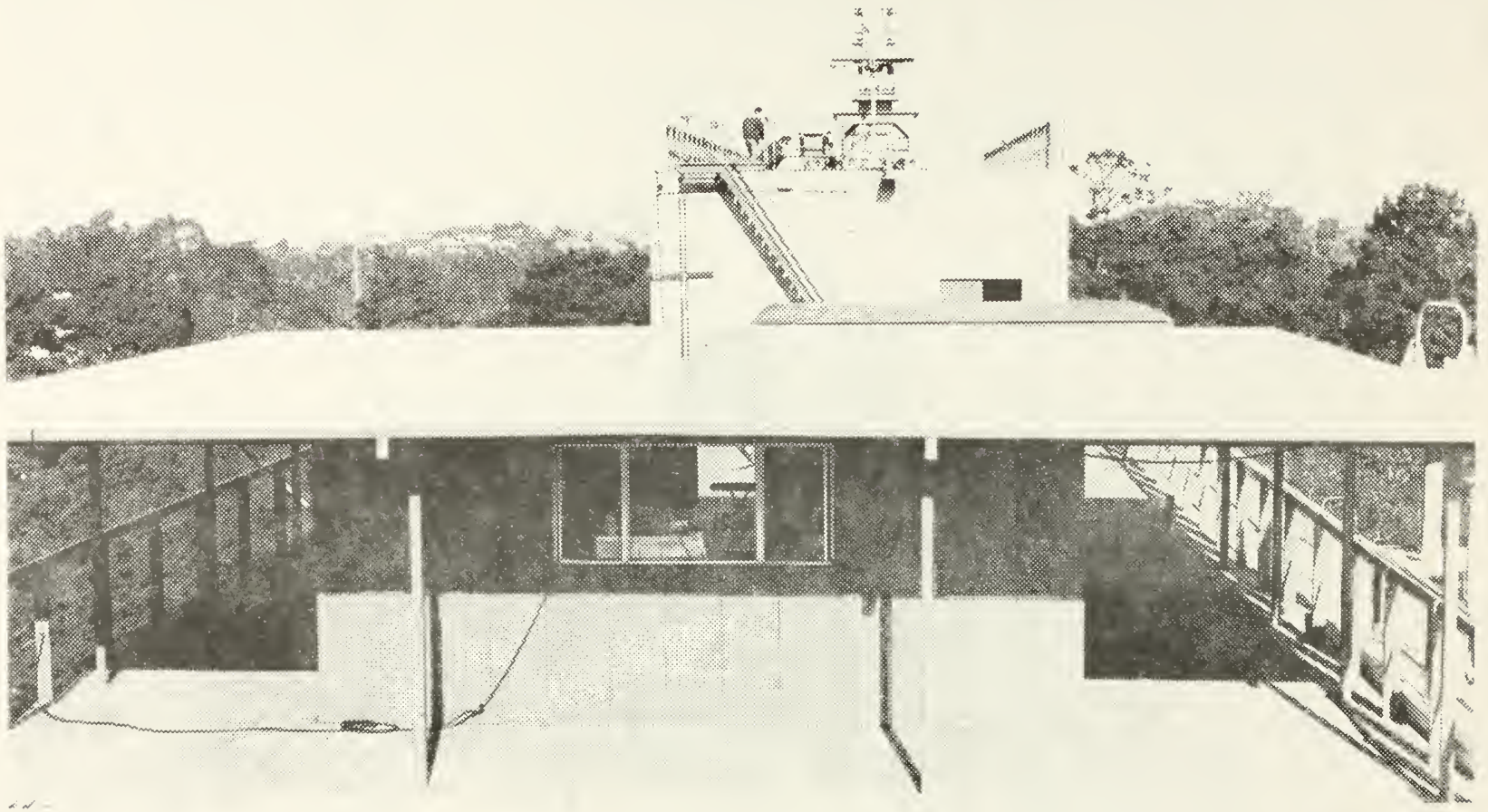

Figure 4. - Image Plane Structure

plexiglass dielectric which provided support for the center conductor.

An aluminum flange at the top of the outer conductor was constructed to recess into an 8 inch hole in the image plane. The hole location was slightly off-center of the image plane surface to minimize the possibility of resonances along the image plane.

Protruding from the center conductor and extending approximately 2.5 inches above the plexiglass support was a brass ring which was machined to the inner diameter of the 2.5 inch brass tube. The various antennas under consideration were slid over this protruding ring. The ring provided support for the antennas.

1. Short Unslotted Feed System

The Short Unslotted Feed System (shown in figure 5) was constructed to permit access , through the interior of the inner conductor, to the uppermost part of the vertical member of antennas considered. To accomplish this the extension below the antenna feed point was relatively short (approximately 42 cm).

The feed system was excited through N-type connectors located approximately 24 centimeters above the base plate (this distance was found not to be critical). The center conductor of the connectors was extended by 1/8 inch brass

rod which made contact with the inner conductor of the feed system. The outer conductor was terminated on the outer conductor of the feed system.

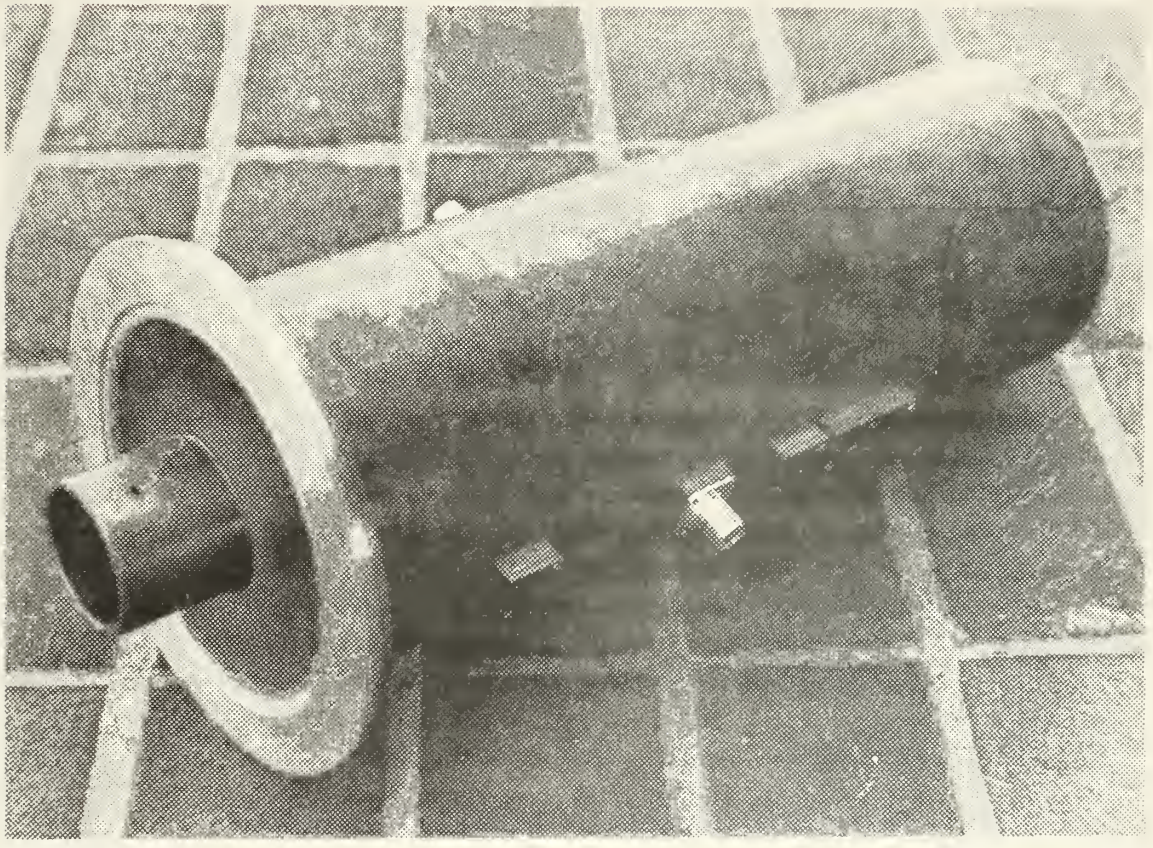

Figure 5. - Short Unslotted Feed System

The outer diameter of the inner conductor and the inner diameter of the outer conductor was measured as 6.37 and 14.9 cm respectively. From these measurements the characteristic impedance of the line was determined as follows:

$$Z_c = [138/(\varepsilon_r)^{1/2}] \log(D_o/d_i) = 50.9 \text{ ohms},$$

where "D_o" and "d_i" were the outer and inner conductor diameters respectively and ε_r, the relative dielectric constant, was equal to 1 (air dielectric).

2. Long Slotted Feed System

The Long Slotted Feed System was used for determination of the antenna input impedance. Construction was essentially the same as that for the short system. The length was extended to 126 cm (the excitation point location remained approximately 24 cm above the base plate) and a 1/8 inch slot was cut axially in the inner conductor, extending from the feed system excitation point to the antenna feed point. The six inch brass tubing was selected with 1/8 inch wall thickness, vice the 1/16 inch used for the short system, to provide additional support. This resulted in a decrease of the inner diameter of the outer conductor to 14.6 cm and a corresponding change in the characteristic impedance to 49.7 ohms from 50.9 ohms obtained for the short system.

C. ANTENNAS

Two and one-half inch brass tubing was used to construct the antennas herein discussed. The lower end of the tubing forming the antenna was open permitting it to slide over the brass ring protruding from the feed system, the antenna thus formed an extension of the inner conductor of the feed system above the image plane.

1. Monopole

The basic monopole was 101.5 cm in height with a 1/8 inch slot cut axially from 30 cm to 100 cm above the ground plane. A long slot cut in brass tubing in this manner has a tendency to spread open at its unsupported center. The slot in this monopole had spread to a maximum width of 1/4 inch at its midpoint, tapering to 1/8 inch at the ends. The problem of slot spreading was corrected when the long feed system was constructed by placing 1/8 inch brass rods across the inner diameter of the tube. These rods were fitted into counter sunk holes in the tube and soldered in place. The external surface was machined to restore the contour.

2. Crossed-Monopole

The basic cross structure from which the desired antenna configurations were constructed consisted of a vertical member 99 cm high with a cross arm 62 cm long, extending equally on either side of the vertical member, and

fixed to the vertical member such that its center was 68.4 cm above the ground plane. Two sets of 1/8 inch slots were cut into the cross. The slot cut axially in the vertical member equidistant between the arms and its perpendicular extension onto one arm was referred to as the surface slot. From this slot the primary charge and current distribution measurements were taken. The other set, consisting of an axial slot on the vertical member which passed under one arm and a joining slot out the arm on the under side, was called the axillary slot. One configuration of a crossed-monopole above an image plane with both the surface and axillary slots visible is shown in Figure 6. The vertical slots extended from approximately 30 to 98 cm above the ground plane. The horizontal (arm) slots originated on the vertical member and extended to 30 cm from the center of the vertical member.

3. Length Adjustment

To adjust the physical height of the antenna and the length of the arms various extension pieces, also constructed of 2.5 inch brass tubing, were fitted onto the open ends of the members. They were held in place by thin brass rings machined to the inner diameter of the 2.5 inch tubing and slotted to provide spring tension.

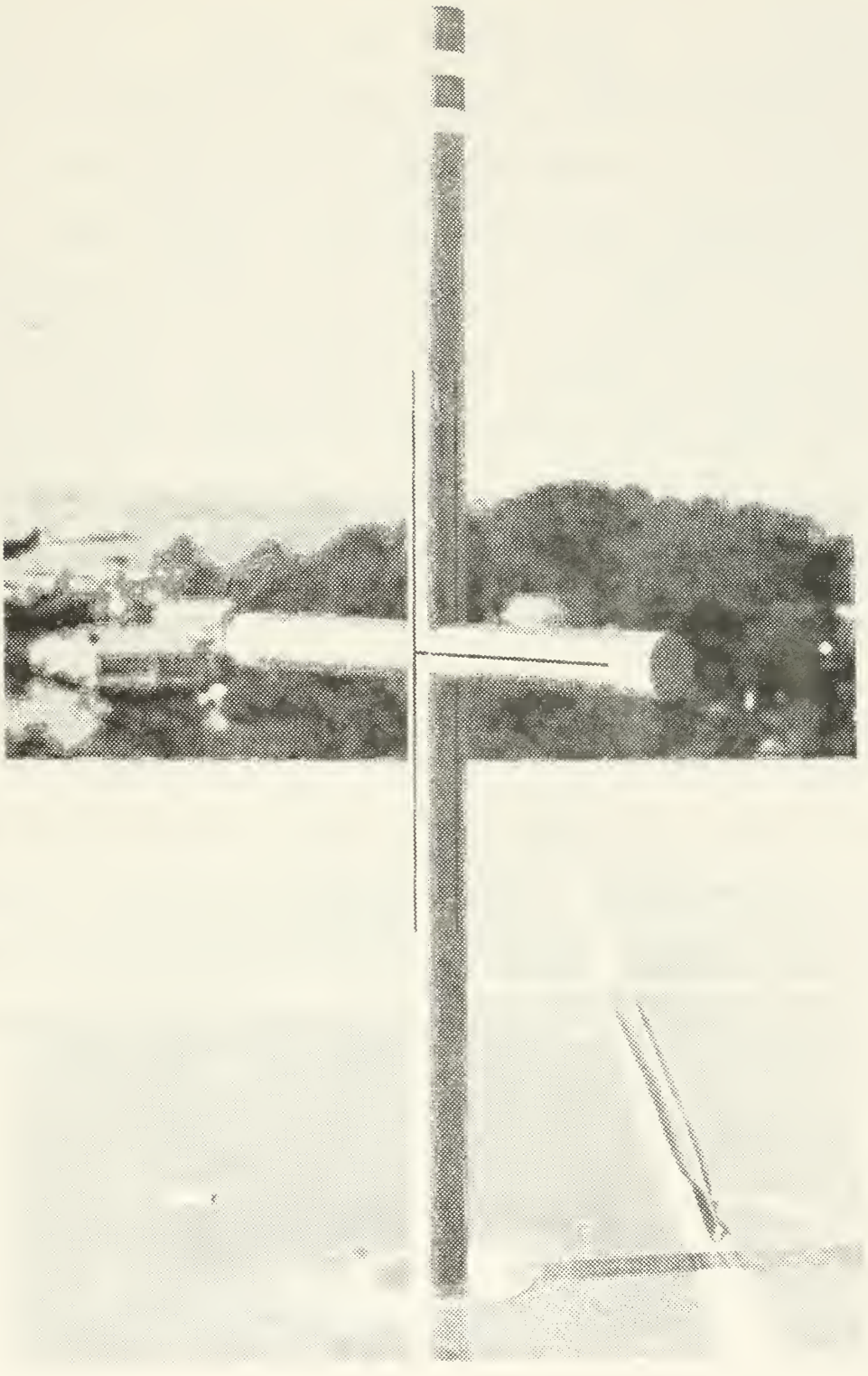

Figure 6. - CASE 4 Crossed-Monopole

For convenience the extension pieces were a variety of lengths (25, 7.5, 5, and 3.25 cm). Minor additional adjustments in length were accomplished by sliding the extension pieces on the brass rings. Discontinuities in the surface were closed with "MACTAC" conducting aluminum or copper tape, which provided additional support for the extensions and fixed them in position. Since the surface irregularities were small with respect to wavelength and were not in the immediate measurement area, they had no effect on the observed charge and current distributions. The tape served mainly to physically restrain movement of the extensions.

End caps were used to close the upper end of the vertical member and the outer ends of the arms. They added .3 cm to the length of the member when not slid out to otherwise adjust the member length. Four extension pieces of various lengths and an end cap (lower center) are shown in Figure 7.

Figure 7. - Extension Pieces and End Cap

D. CHARGE AND CURRENT PROBES

Sampling of the radial E and the tangential H fields in the near vicinity of a conductor provides the basis for experimental determination of the surface charge and current distributions respectively on the conductor. The sampling device must meet three general requirements: (1) its relative electrical size must be sufficiently small that the induced voltage or current in the sampling element can be attributed to a section of conductor very short compared with a wavelength; (2) it must also be located close to the

conductor to satisfy the above condition; (3) it must be loosely coupled to the field of the conductor to minimize the disturbance of the charge and current distributions, which requires that it be sufficiently sensitive [King 1956]. An insulated linear monopole charge probe and a singly loaded, shielded, circular loop current probe satisfied the above three conditions and were used for the measurements included herein. The probes used are shown in Figure 8.

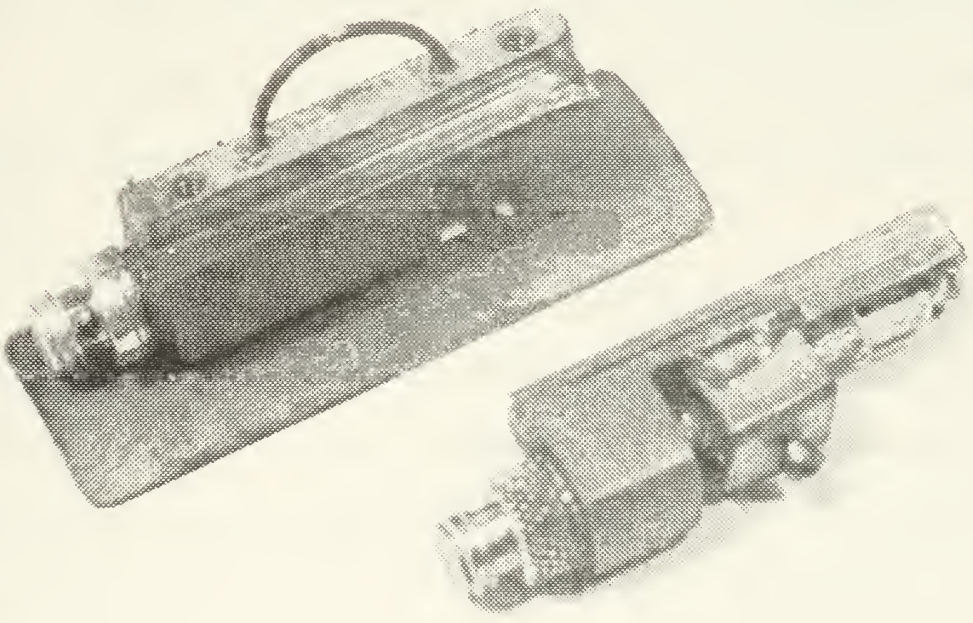

Figure 8. - Charge and Current Probes

1. Design and Construction

The current probe sensing element was constructed of solid shield (UT - 20) coaxial cable with .02 inch outside diameter, .005 inch o.d. center conductor, and a Teflon dielectric. The element was semicircular with a radius of .5 cm. The outer conductor and dielectric were removed forming a gap of .02 cm at the midpoint of the arc. The dielectric and center conductor were removed from the shield on the side of the arc remote from the connector. The shield over this part of the arc was filled with solder. The probe element shield was soldered to the brass probe body at both ends of the arc. The center conductor was led to a Microdot 31-34 connector mounted in the probe body through which the measurement equipment was joined to the probe.

Construction of the charge probe was essentially the same as for the current probe. The charge sensing element consisted of a 1.7 cm segment of Microdot Microminature (250-3920) coaxial cable protruding perpendicularly from the probe body from which the outer conductor had been removed.

The probe body was machined to recess into the 1/8 inch slots in the antenna members placing the probe sensing element on the outside of the antenna (center conductor in the case of the long slotted feed system). Figure 9 shows

the beryllium copper retainer plates which were placed over the sensing element and attached to the probe body holding it in the slot under slight spring tension, but permitting it to be moved axially.

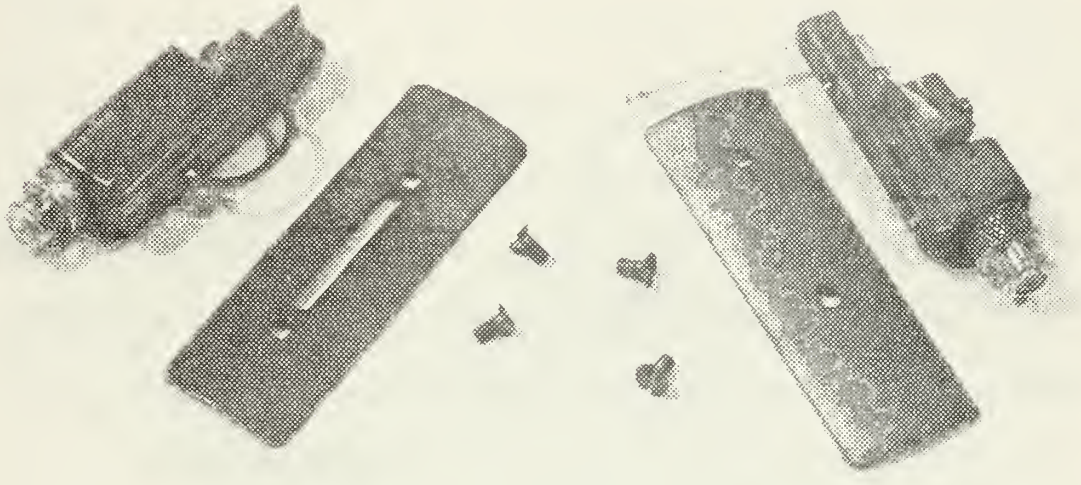

Figure 9. - Charge and Current Probes with Retainer Plates

2. Connections

A section of RG 142 B/U double shielded cable from which the shields had been removed was fed through a 150 cm length of 1/8 inch brass tubing which had a Microdot 32-21 connector soldered in the end. The Mircrodot connector had been modified to accept the RG 142 B/U cable. The shields of the remaining portion of the RG 142 B/U cable were soldered to the opposite end of the brass tube. The brass tube (probe rod) thus formed a 150 cm rigid extension of the outer conductor of the RG 142 B/U cable which was terminated

in a Microdot connector acceptable to the probe. The opposite end of the shielded cable was terminated in an N connector. The above connection arrangement served to connect the probe with the measuring instrument for all vertical measurements.

For horizontal (arm) measurements a 146 cm length of flexible, shielded, Microdot Microminature (250-3920) coaxial cable with appropriate connectors was attached between the probe rod and the probe. Pullies were located within the interior of the antenna at the junction such that they guided the flexible cable to the arm slot location without undue friction.

3. Positioning

Attached to the base plate of the feed system was a rack and pinion with a pointer attached to the movable pinion housing and a metal metric scale attached to the fixed rack. The probe rod, which protruded from the interior of the center conductor of the feed system through the base plate, was attached to the pinion housing by 4 screws through a holding plate. Figure 10 shows the positioning mechanism.

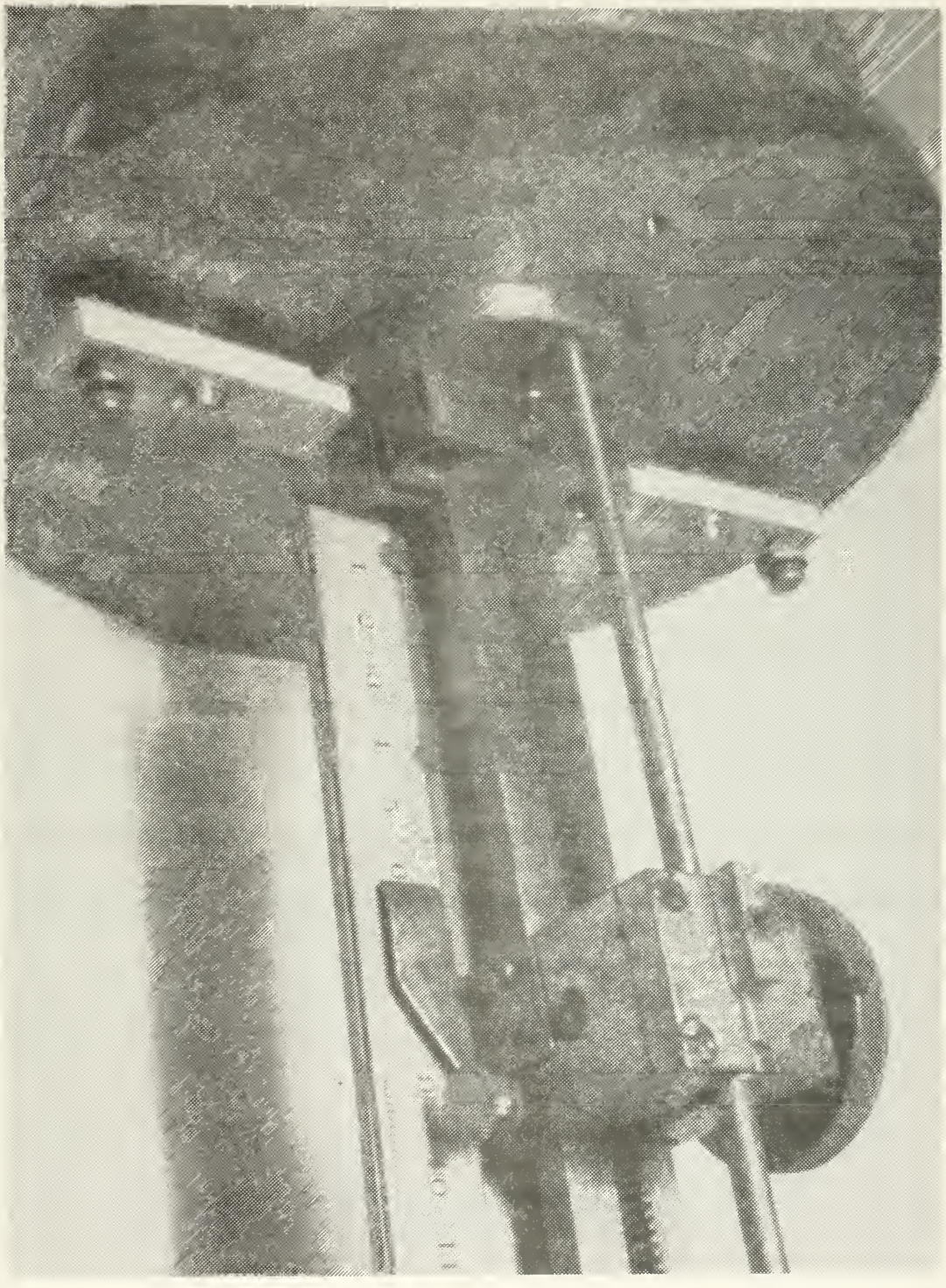

Figure 10. - Rack and Pinion Probe Positioning Mechanism

For all vertical measurements the knurled knob (attached to the pinion) was turned to drive the probe up and down in the vertical slot. By this method the probe was accurately located within ± .01 centimeter of the desired position.

To position the probes while taking arm measurements a strand of monofilament line (in addition to the flexible cable) was led through the junction pulley which alligned with the desired slot. One end of the monofilament was attached to the probe body; the other end was led out through the base plate opening and attached to the pinion housing.

The probe was first located at its extreme radial position. The positioning mechanism was then used to draw the probe along the arm slots toward the vertical member. Irregularities in the slot surface and stretching of the monofilament line detracted from the accuracy of positioning for these measurements. Possition error was not greater than ± .1 centimeter.

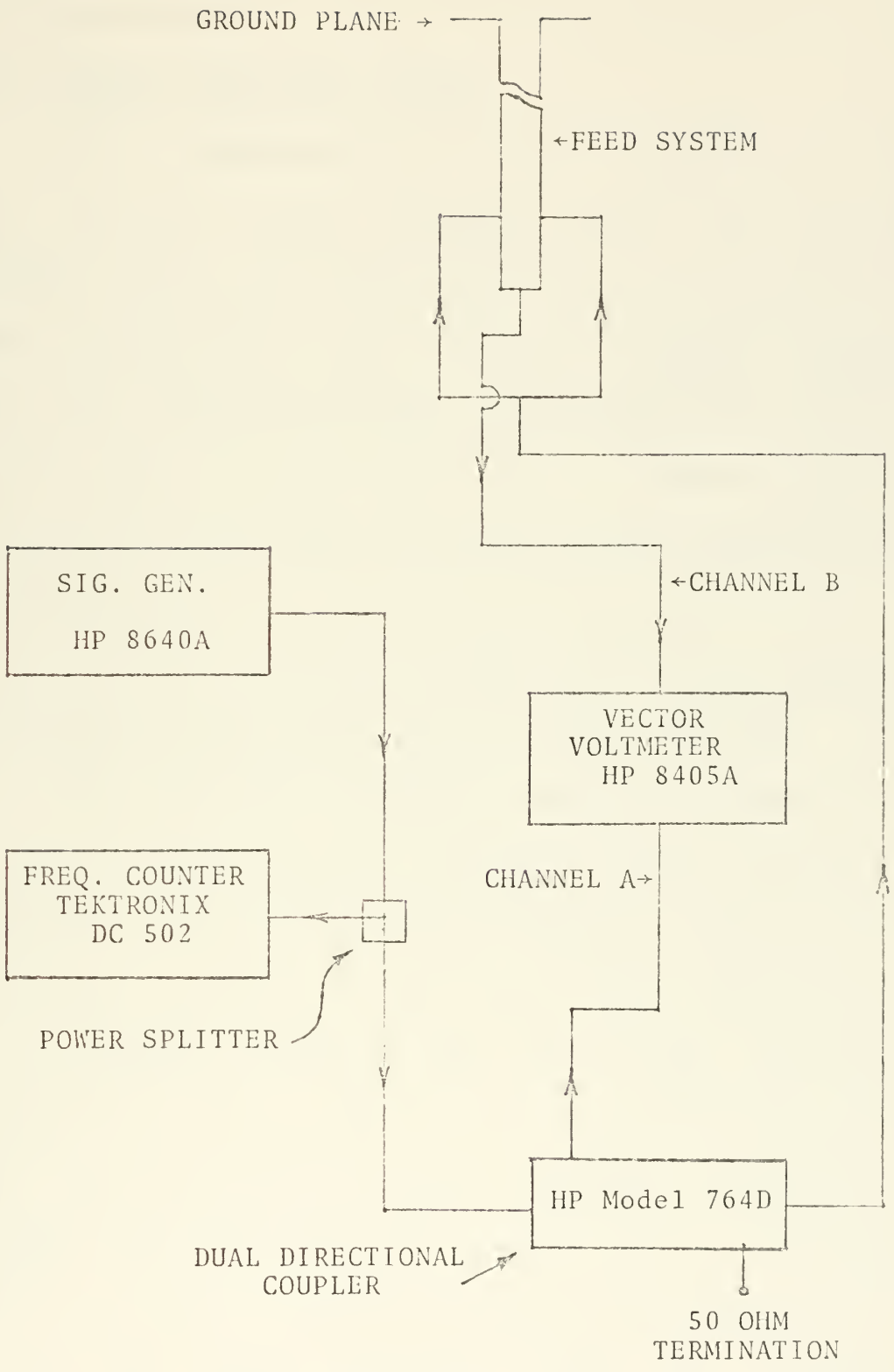

Figure 11. - Block Diagram of Instrumentation

E. INSTRUMENTATION

1. Antenna Excitation System

Basic considerations for the selection of the antenna excitation system equipment were: (1) to have sufficient power that the measured data was stable and not subject to interference; (2) to have a stable frequency source; (3) to have available to the measurement system a reference signal for phase measurement. A block diagram of the instrumentation which satisfied these requirements is shown in Figure 11.

The output from a Hewlett Packard 8640A signal generator was divided by a HP 11549A type N power splitter. One output from the power splitter provided a sample of the signal to a Tektronix DC 502 frequency counter which was monitored to assure frequency stability over the period of measurements. The second output of the power splitter was led to a Hewlett Packard Model 764D dual directional coupler. The direct output from the dual directional coupler was divided by an N type T connector and applied to the antenna under consideration through the N connectors located on opposite sides of the antenna feed system outer conductor. The signal reflected from the impedance mismatches in the feed line was isolated by the dual

directional coupler and dissipated in a HP 908A 50 ohm termination.

A reference signal for phase measurement was obtained from the attenuated forward output of the dual directional coupler through a HP 11536A 50 ohm tee (type N to probe) to which a HP 908A 50 ohm termination was connected. A fixed power level was obtained for the measurements by noting the reference signal level for 10 dbm at the direct output of the dual directional coupler with the coupler terminated in a matched load. The reference signal level was measured for each frequency used and was re-established by adjusting the signal generator output for subsequent measurements.

2. Measurement System

The heart of the measurement system was the Hewlett Packard Model 8405A Vector Voltmeter. This instrument has a voltmeter and phasemeter for directly measuring the amplitude and phase relationship of the fundamental components of two RF voltages. The reference signal, obtained from the attenuated forward output of the dual directional coupler, was applied to Channel A of the vector voltmeter. Channel B was connected to the charge or current probe through a HP 11536A 50 ohm TEE and the RG 142B/U cable. The magnitude of the signal present on the probe lead was read from the voltmeter while the phase of the

signal, with respect to the reference signal, was determined from the phasemeter. The table top arrangement of the instrumentation in the ground plane was as shown in Figure 12.

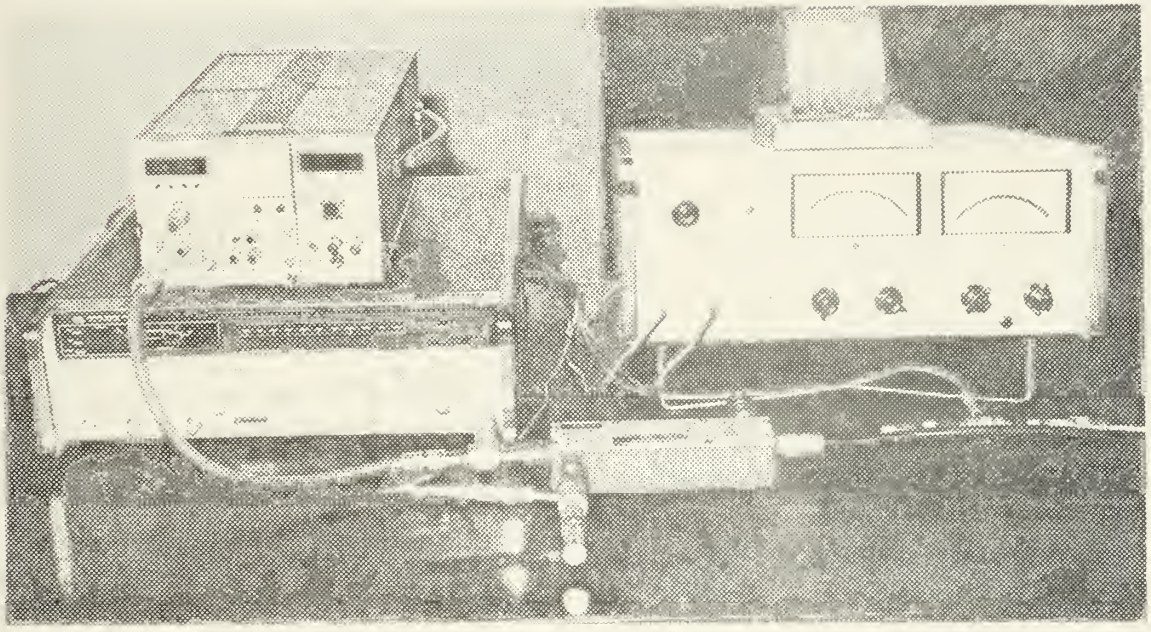

Figure 12. - Arrangement of Instrumentation

3. Accuracy

As previously mentioned the possitioning accuracy of the probes was within ±.01 centimeter for vertical measurements and within ±.1 cm for arm measurements. Observation of the frequency counter permitted the frequency to be held within ± 1 kHz. At the frequencies used the voltmeter accuracy was ±6 percent of full scale. Phase accuracy of the vector voltmeter at a single frequency, with equal voltages applied to channels A and B is ±1.5 degrees;

however, the voltages over the range of measurements were not equal. The worst case of ±4.5 degrees must be accepted. Bandwidth of the vector voltmeter is 1 kHz. This narrow bandwidth virtually eliminated interference resulting in very stable data. Noise pick-up by the probes at both charge and current minimums was not detectable.

IV. EXPERIMENTAL PROCEDURE

A. DATA ACQUISITION

Prior to recording data the signal generator, frequency counter, and vector voltmeter were permitted a warm-up period of approximately 2 hours. This was found to eliminate an undesirable phase drift observed with insufficient warm-up time. The "zero height" of the probe was established by positioning it at its highest (98.4 cm above the ground plane) or greatest radial (26.8 cm from the vertical center) position, depending on whether vertical or arm data was to be taken, and adjusting the pointer on the pinion housing to read zero (highest scale position) while sliding the probe rod through its mounting. The probe rod holding plate was then tightened down fixing the height of the probe at zero scale reading. This height was recorded for later use in the conversion of scale reading to probe position. The power applied to the antenna was adjusted to the reference level previously descussed. With this, the preliminary adjustments of the system were complete, and data could be recorded.

Actual data taking consisted of adjusting the probe position (usually in 1 cm increments), and entering in the

log the scale reading, voltmeter reading, and the relative phase from the phasemeter for each position.

B. DATA PROCESSING

Data from the log was manually entered into the memory of the Hewlett Packard 9821A Calculator. Once in memory, the data was recorded on magnetic tape from which it could be efficiently re-entered into memory for processing and plotting.

Eighty current and 80 charge data points, each point consisting of a position, magnitude, and phase element, could be stored in active memory leaving sufficient registers for the plotting/processing program and allowing 20 memory registers for identifying information and program use. This number of data points was not an absolute limit for this system. Other programs could be devised which would call subprograms or data from magnetic tape thus increasing the data storage capability; however, 80 data point storage locations was adequate for the data presented herein.

Data processing included converting the scale readings into probe position, applying various corrections (as discussed in the following section) to the magnitude and phase values, and scaling the magnitude for plotting. Once

converted, corrected and scaled the data was plotted on the companion HP 9862A Plotter which, with the HP 9821A calculator forms the calculator/plotter system shown in Figure 13.

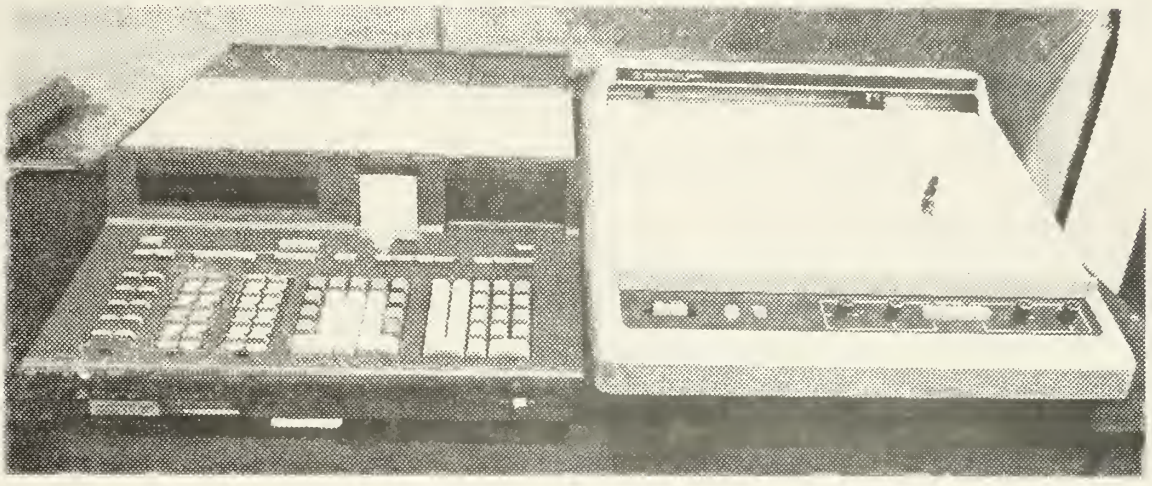

Figure 13. -

Hewlett Packard Calculator-Plotter System

C. DATA CORRECTIONS

Probe calibration is required to ensure that experimental results are in agreement with known parameters and that results obtained with various systems are consistent. Since both magnitude and phase are recorded from the probes, consideration must be given to the adjustment of each.

1. Phase Calibration

From transmission line theory it is known that in a lossless line the positions at which voltage is maximum and current is minimum and vice-versa are those at which zero relative phase exists between these quantities. It is also known that within odd quarter-wavelengths from a short in a transmission line the impedance seen across the line is a pure inductance while within even quarter-wavelengths the impedance seen is purely capacitive. This theory provided one parameter, a known relationship between the charge and current phase at specific points within the feed system, to assist the calibration.

It was decided to investigate the charge and current distribution data within the long slotted feed system, shorted at the image plane surface, in an attempt to establish a phase calibration factor. Two frequencies (195 and 300 MHz) were used to scale element length such that a charge maximum or minimum would occur at the proposed junction in investigations of the crossed-monopole (as later discussed). It was anticipated that different calibration factors would be required at each frequency.

Charge and current data was taken at both frequencies within the shorted feed system and plotted. In addition, the charge magnitude divided by the current magnitude; and,

the charge phase minus the current phase were plotted at each data point. Since charge magnitude at a point within the feed system is proportional to the voltage across the feed system at that point, the charge magnitude divided by the current magnitude was proportional to the magnitude of impedance seen at the data point. Charge phase minus current phase at a point in the system yielded the angle of the impedance seen at that point.

The parameter being calibrated was a relationship between charge and current phase and not an absolute value of either quantity, it was therefore not necessary to scale both values. It was decided to apply the phase calibration factor to the current phase only. From the graphs it was determined that the current phase calibration factors required to adjust the impedance angle to +90 degrees within odd quarter-wavelengths of the short and -90 degrees within even quarter-wavelengths of the short were +5.5 and +12 degrees at 195 and 300 MHz respectively. It will be seen that the requirement for charge and current to be in phase at voltage maxima/current minima and current maxima/voltage minima was satisfied by application of these factors.

The calibrated plots of the charge and current distributions within the shorted feed system at 300 and 195 MHz are shown in Figures 14 and 15 respectively. Details of

the graph format will be presented in a later section. At this point it should be noted that charge magnitude and charge phase have been labeled $|V|$ and Θ_V respectively. This labeling will be discussed more fully in the following section, but essentially results from an assumption of 1 volt across the feed system at the charge maximum. The height axis zero occurs at the short in these figures.

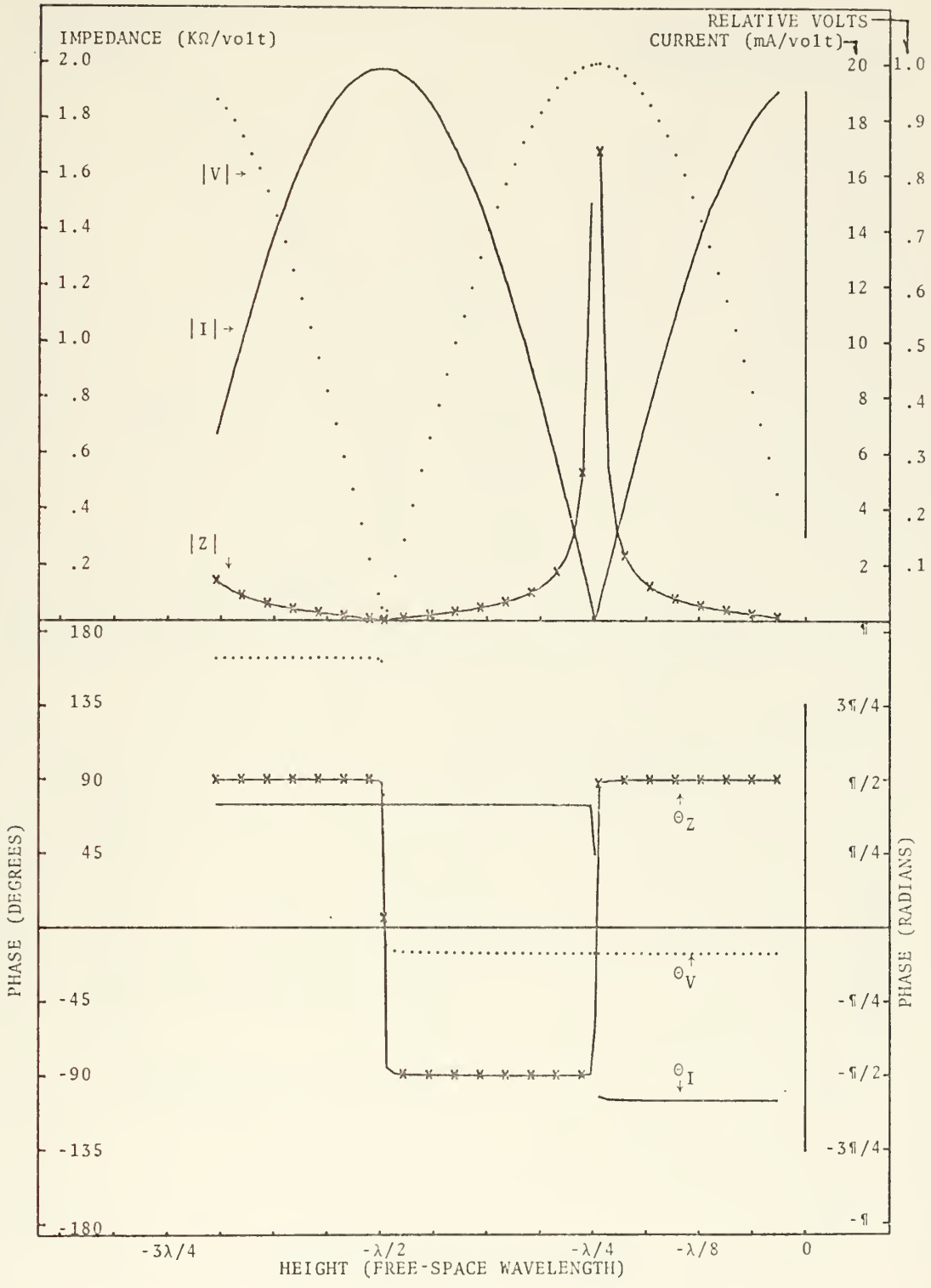

Figure 14. -

Measured charge and current, and calculated impedance at 300 MHz (relative to 1 volt at maximum charge) within a coaxial feed system terminated in a short circuit.

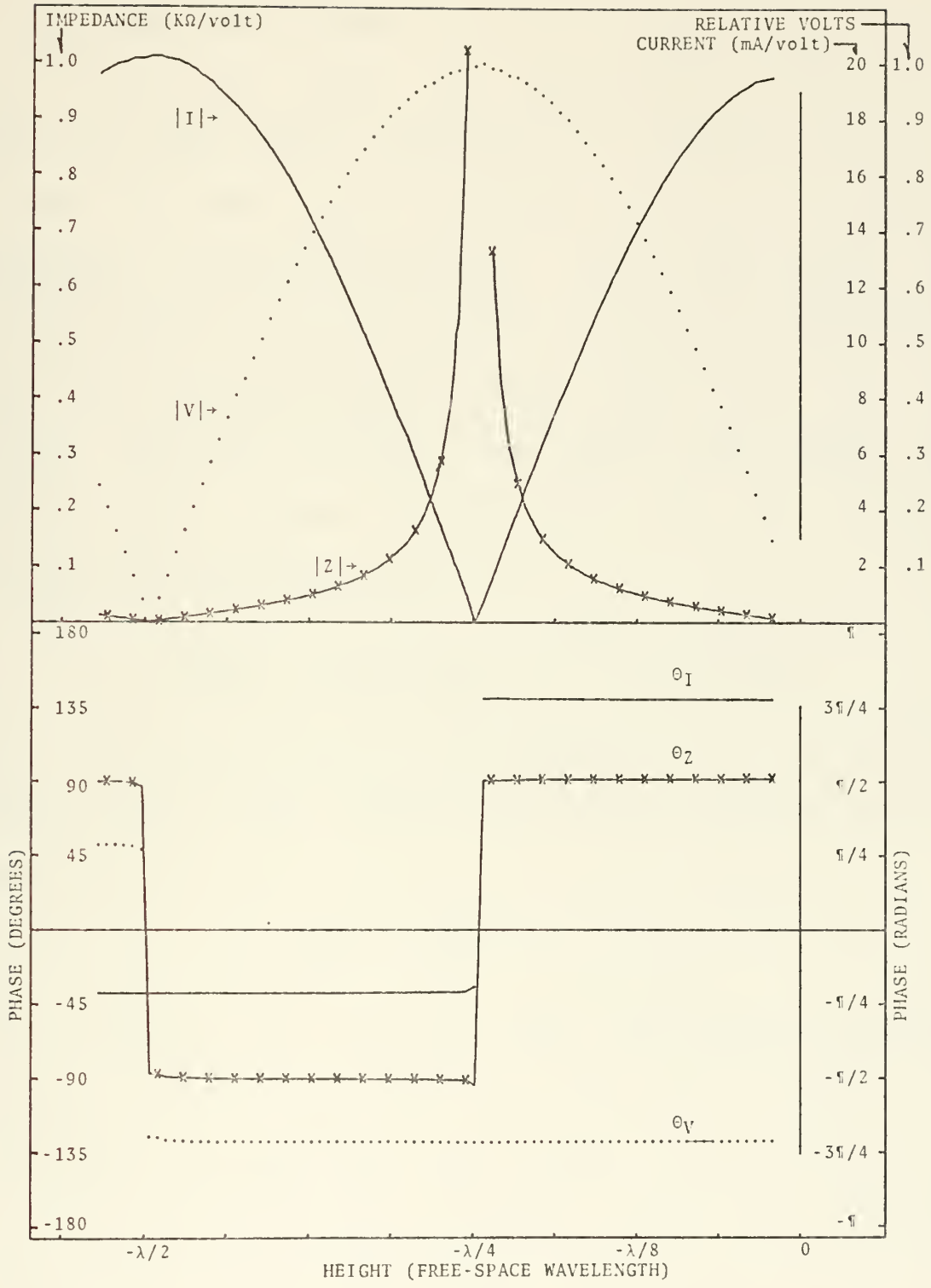

Figure 15. -

Measured charge and current, and calculated impedance at 195 MHz (relative to 1 volt at maximum charge) within a coaxial feed system terminated in a short circuit.

2. Feed System Plots

Plots of current and charge probe magnitude data within the feed system terminated in an impedance other than a short or open circuit yielded the key to meaningful adjustment of the probe magnitude. From these plots the Voltage Standing Wave Ratio (VSWR) was evident. The VSWR is equal to the charge magnitude maximum value divided by the charge magnitude minimum value where the constant of proportionality between charge probe data and voltage cancels out of the equation:

$$VSWR = |V_{max}| / |V_{min}| = K|\rho_{max}| / K|\rho_{min}|$$

From knowledge of the VSWR, the magnitude of the reflection coefficient at the antenna/feed system interface could be obtained:

$$|K_L| = (VSWR-1) / (VSWR+1)$$

By introducing the distance from the apparent impedance maximum along the feed line to the feed point aperture, as read from the data plot, this equation could be solved for the normalized feed point impedance using the normalized transmission line Smith Chart. Application of the feed system characteristic impedance (previously determined) to the normalized feed point impedance yielded the input

impedance of the driven antenna at the ground plane/antenna interface [Brown et al. 1973, p. 66]. This technique was used for later determination of antenna input impedance.

A relationship was now established between current and voltage along the feed system. If the constant of proportionality between the current or charge probe data and the actual current or voltage could be established both probes could be absolutely calibrated. Such was not the case.

It was decided to accept a reference voltage of 1 volt at the charge maximum along the feed system (as later discussed, this was not the optimum choice of reference). With this decision the charge magnitude scale factor was fixed.

$$\text{Charge Scale Factor} = Q_{SF} = 1/|\rho_{max}|$$

Since Q_{SF} normalized the charge magnitude data by scaling, it was also applied to the current magnitude probe data to maintain the relationship between them.

The current magnitude correction factor was chosen as that value which when multiplied times the scaled current data would yield the proper impedance. That is

$$Z = V/I = (Q_{SF}\rho_P)/(I_{CF}Q_{SF}I_P) = P/(I_{CF}I_P)$$

where the subscript P indicates probe values and I_{CF} is the current magnitude correction factor. This factor was graphically determined from the current and charge probe data plots at the point one-half wavelength from the feed aperture. It was assumed that the previously calculated value of feed point impedance was also observed one-half wavelength from the feed point. The current magnitude correction factor was independently determined for each feed system plot.

3. Crossed-Monopole Plots

In the crossed-monopole plots the charge and current distributions on the reference monopole, the vertical element of the cross, and the horizontal element of the cross were to be represented. It was desired that these three presentations be consistent.

The most obvious requirement for consistency was between the arm data and the vertical data where a flexible coaxial cable had altered the measurement system for arm data. To establish the relationship between these two different measurement systems they were used to measure the charge and current distributions on the same monopole. This data was plotted and the factors required to coalesce the curves were graphically determined.

At 300 MHz the factors were:

Charge Magnitude	-	1.080
Charge Phase	-	+27°
Current Magnitude	-	1.165
Current Phase	-	-150°

At 195 MHz the factors were:

Charge Magnitude	-	1.075
Charge Phase	-	+125°
Current Magnitude	-	1.239
Current Phase	-	-53°

Figures 16 and 17 show the graphical results of this technique for 300 and 195 MHz respectively. The subscript U in these figures indicates those curves taken with the arm measurement connections which were uncorrected. Other curves are both the data taken with the vertical measurement system and data taken with the arm measurement system and then corrected. In most areas these curves are not separable. Where two current magnitude ($|I|$) curves are indicated with A and B, the B curve is the corrected current magnitude data (that taken with the arm measurement system).

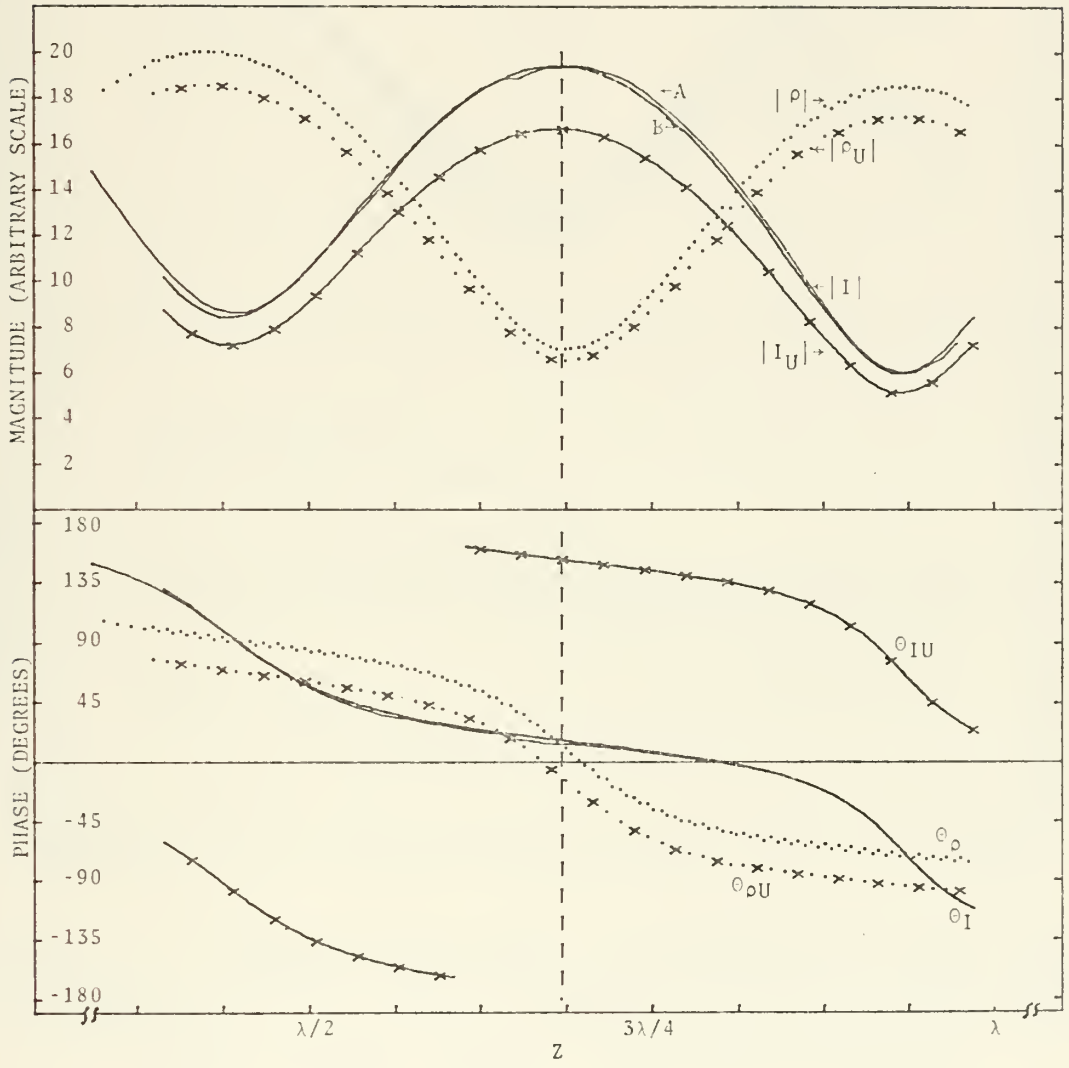

Figure 16. - Measured currents and charges per unit length on a transmitting monopole comparing arm measurenent system with vertical element measurement system.

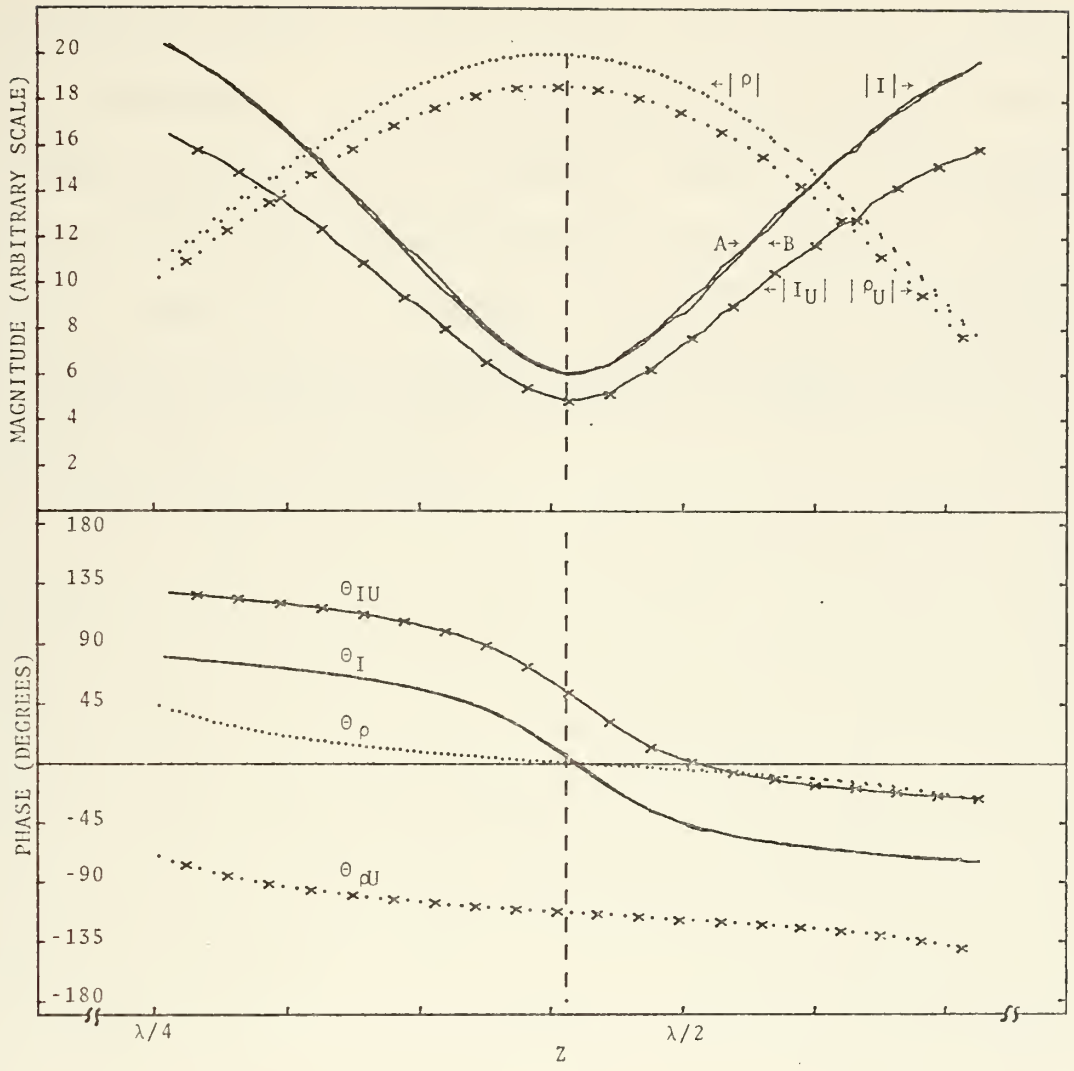

Figure 17. - Measured currents and charges per unit length on a transmitting monopole comparing arm measurement system with vertical element measurement system.

In addition to the correction factors applied to the arm data all charge plots on the crossed-monopole graphs were normalized to the maximum charge value to be plotted. A current magnitude correction factor (the average of those obtained from the impedance plots for the frequency in use) was also used to adjust the current magnitude. This

adjustment was made in the same way as for the impedance plots assuming 1 volt at maximum charge. This technique provided scaling for the currents; however, the magnitude scale on the plots remained "arbitrary" since the notion of 1 volt at maximum charge along an antenna was meaningless. The current magnitude scale factors used were .01776 at 300 MHz and .01710 at 195 MHz.

V. EXPERIMENTAL RESULTS AND ANALYSIS

A. DEFINITION OF CONFIGURATIONS

As previously mentioned, the crossed-monopole configurations investigated herein arise from a superposition of Figures 3 (a) and (b) on Figures 1 (b) and (c). Four configurations arise directly from these superpositions. The fifth considers a non-symetric horizontal element with one arm resonant, the other antiresonant.

In Figure 18 the dimensioning of an arbitrary crossed-monopole is shown. The origin of the X-Z plane in which the cross is shown is at the antenna/image plane interface. Four conductors are connected to produce 4 mutually perpendicular, confluent members with lengths h_1, h_2, l_1, and l_2 with a common junction at $x = 0$, $z = h_1$. The height of the vertical element is h ($h = h_1 + h_2$); the total length of the horizontal element is l ($l = l_1 + l_2$).

The first crossed-monopole configuration considered (CASE 1) was to have resonant vertical elements, producing a charge minimum at the proposed junction, and antiresonant horizontal arms. A frequency of 300 MHz was selected to

achieve a resonant length (n = 3 in: Length = n $\lambda/4$) consistent with the fixed dimension (h_1) of the basic cross and the shortening of wavelength on the reference monopole. The length h_2 was then chosen equal to h_1 for symmetry to eliminate the effects of uncanceled forces on charge in the arms (previously discussed). Lengths l_1 and l_2 were chosen as that fraction of the height (h) which would be antiresonant.

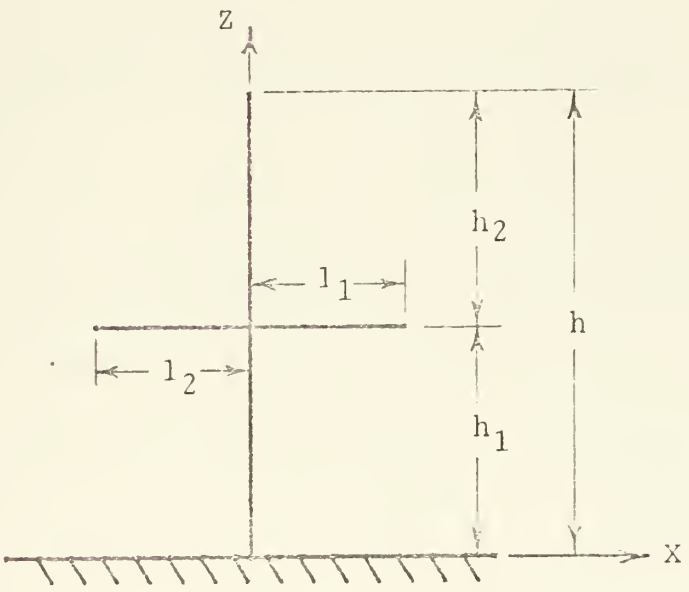

Figure 18. - Dimensioned Arbitrary Crossed-Monopole

For CASE 2 the process of selection of element length was the same as that for CASE 1 except that the arms were chosen as that fraction of the height (h) which would be

resonant. Since the fixed length of the slotted arm on the basic cross exceeded 1/4 wavelength, the 3/4 wavelength resonant length was chosen.

For the remainder of the cases considered antiresonant vertical elements were desired to present a charge maximum at the proposed junction. Frequency scaling was used to "shorten" the fixed length h_1 of the basic cross to the first antiresonant length. The frequency at which this was achieved was 195 MHz. CASE 3 was that configuration which joined equal antiresonant arms to the point of charge maximum on the reference monopole, while in CASE 4 the equal arms were resonant.

For CASE 5 the junction was to remain at the charge maximum of the reference monopole, but the arms were to be unequal (one resonant, the other antiresonant). Since only one arm of the basic cross was slotted, data could only be taken from one arm of the configuration. The data arm was designated as l_1. This case was then subdivided into two cases such that the data could be accumulated from both the resonant arm (CASE 5A) and the antiresonant arm (CASE 5B).

Figure 19 shows the various cases considered. Element length is shown as a fraction of free-space wavelength.

Cases 1 and 2, and cases 3, 4, and 5 were scaled to the same physical height in this figure as were the actual crossed-monopole antennas.

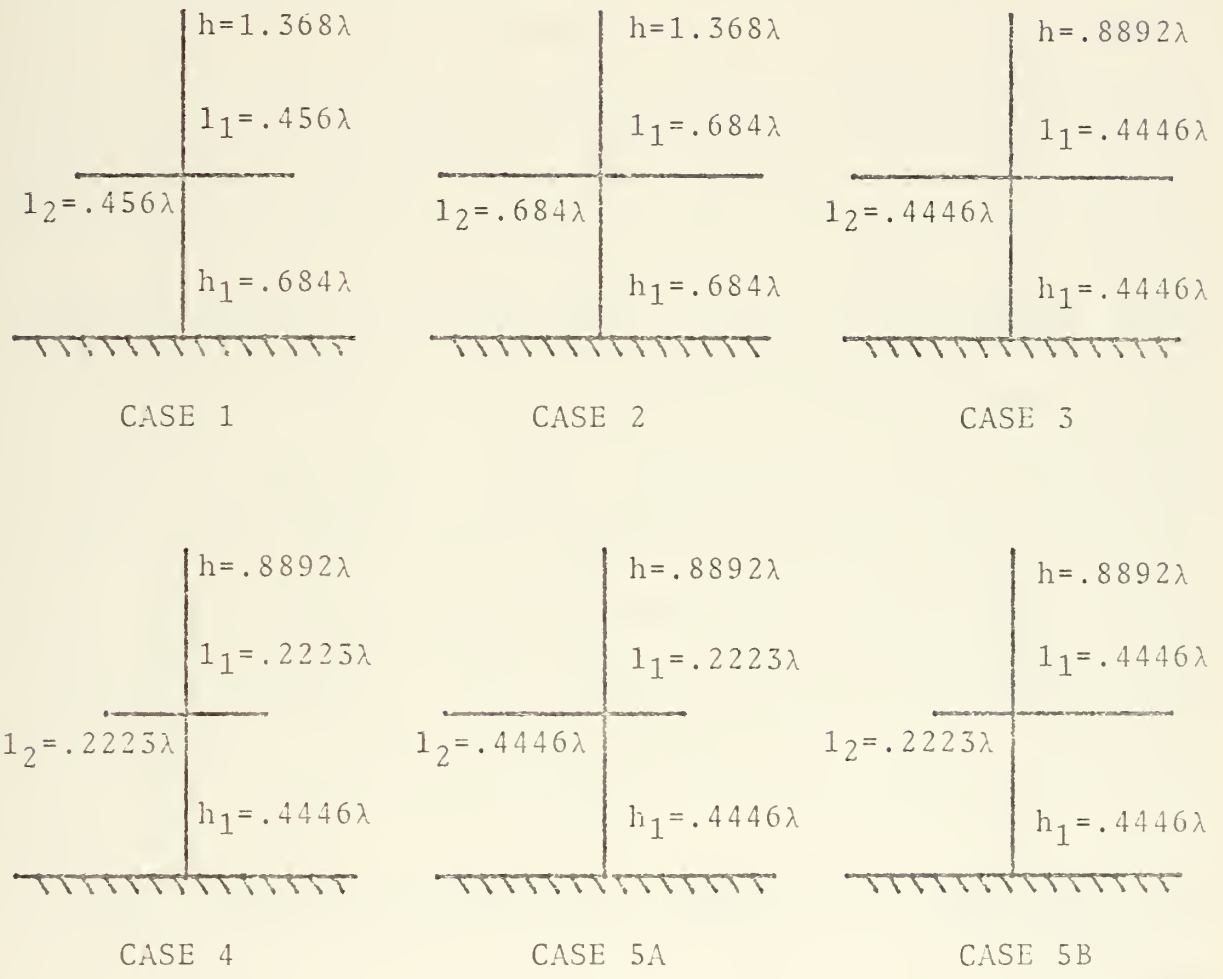

Figure 19. -
Illustration of Crossed-Monopole
Configurations Investigated

B. INPEDANCE MEASUREMENTS

1. Feed-Point Correction

The feed system described earlier resulted in an annular gap in the image plane surrounding the vertical antenna with an outer radius (b) of 7.3 cm and an inner radius (a) of 3.185 cm. The antenna is driven by fields in this annular region and the input impedance is defined here. The driving point of the antenna, however, is not well defined since the driving field is axially distributed over the center conductor a distance approximately equal to the conductor separation. This distribution of the driving field results from the introduction of higher order modes of excitation to the normal TEM mode of the coaxial line by the coupling effects of the antenna with the line and the nonuniformity of the capacitance per unit length near the end of the line.

The voltage standing-wave measurement technique for determining the driven antenna apparent input impedance described in section IV.B.2. assumes TEM excitation of the coaxial line to the feed point aperture. It is not normally a satisfactory approximation to assume that the apparent admittance as measured back one-half wavelength on the feed line is equal to the actual current per volt entering the antenna. Terminal-zone effects must be considered.

The apparent impedance (Z_a) of an antenna with a small base separation may be expressed in terms of the impedance of an antenna with zero base separation (Z_o) by applying a terminal-zone correction to Z_a, or vice-versa. This correction can be accomplished by letting an assumed lumped series inductance and an assumed lumped shunt capacitance (C_t) replace the feed aperture. The impedance of these lumped elements when combined with the theoretical impedance of the antenna with zero base separation yields the apparent impedance of the antenna. It has been shown [King 1956, p. 65-66] that the series inductance assumed in this manner is approximately zero for a base driven antenna over a conducting plane. The terminal-zone capacitance (C_t) for this arrangement has been calculated and may be obtained from Figure 10.9 of Theory of Linear Antennas [King 1956] where $-C_t/c_o b$ is plotted as a function of b/a.

For the long slotted feed system described herein

$$b/a = 2.29$$

With this value the above referenced figure yields:

$$-C_t/c_o b = .194$$

where c_o is the capacitance per unit length of an infinite line.

$$c_o = \varepsilon_r \varepsilon_o / \ln(b/a) = 33.57 \times 10^{-12} \text{ F/m}$$

for the long slotted feed line considered herein. The terminal-zone capacitance is now determined:

$$C_t = -.194 c_o b = -.475 \times 10^{-12} \text{ F.}$$

Another lumped, shunt capacitance (C_d) resulting from the dielectric support at the feed aperture may be combined with the terminal-zone capacitance to further correct the theoretical impedance for feed aperture effects. The capacitance of the particular dielectric support used herein is determined as follows:

$$C_d = \frac{2\pi\varepsilon_r \varepsilon_o l}{\ln(b/a)} = 1.627 \times 10^{-12} \text{ f.}$$

where $\varepsilon_r = 2.55$ for polystyrene and l is the thickness of the dielectric support.

The susceptance of these lumped capacitances,

$$B_c = 2\pi f(C_t + C_d),$$

is 2.17 and 1.41 millimhos at 300 and 195 MHz respectively. These values may be added to the appropriate theoretical

admittances (Y_o) to yield the apparent admittance (Y_a), or subtracted from the apparent admittances to yield the theoretical admittance:

$$Y_a = G_a + jB_a = G_o + j(B_o + B_c)$$

or

$$Y_o = G_o + jB_o = G_a + j(B_a - B_c)$$

In either case the conductance (G) is seen to be independent of the feed point aperture when the aperture is treated as lumped circuit elements. For this reason later discussion will focus on admittance with particular attention to conductance which is not critically dependent on the experimental set-up.

Noting that the signs of C_t and C_d are opposite, the effects of the terminal-zone capacitance and the dielectric capacitance are off-setting. With careful selection of the material and thickness of the dielectric support, the terminal-zone effect could be canceled by the effect of the dielectric support.

2. Display Format

Graphs of the measured charge and current distributions and the calculated impedance at each data point within the feed system are in two parts. The upper portion being the magnitude of these quantities, the lower portion the phase. Position within the feed system (negative Z direction) is indicated by negative values of height as a function of free-space wavelength along the common abscissa the origin of which occurs at the feed aperture.

Curves representing voltage magnitude (labeled $|V|$) and phase (labeled Θ_V) consist of adjusted charge data plotted as points. Current magnitude ($|I|$) and current phase (Θ_I) curves are plots of adjusted current data with the points connected by straight line segments. The adjustment process for these curves did not include smoothing. Minor irregularities, though unexplained, do not significantly detract from the data. At each data point the calculated impedance magnitude ($|Z|$) and phase (Θ_Z) is plotted. These points are connected by straight line segments on which the approximate position of every third point is marked with an "X" to distinguish these curves from the current curves.

Magnitude scales are separately indicated for each parameter. Relative impedance values are shown on the scale at the left. Relative current in milliamperes per volt and relative voltage scales are indicated at the right. Phase is plotted between ±180 degrees and may be read in degrees from the scale at the left or in radians from the scale at the right.

3. Monopoles

Measurement of the impedance of monopoles was attempted for two purposes: (1) to establish the input impedance of the reference monopoles against which the measured impedances of the crossed-monopoles could be compared; and (2) to assure that the results obtained with the measurement technique used herein were compatible with the theoretical and experimental data available.

a. Comparison With Theory

Monopole heights were selected such that Ω, where

$$\Omega = 2\ln(2h/a),$$

would be compatible with tabulated King-Middleton second-order solutions for impedance, and such that at the frequencies used $\beta_o h$ was within the tabulated range.

At 300 MHz a monopole height of 52.8 cm was selected.

This established Ω at 7.00 and $\beta_o h$ at 3.3175 Both values within the range of tabulated values of the King-Middleton solutions.

The charge and current distributions within the slotted feed system terminated in the 52.8 cm monopole and excited at 300 MHz were measured and plotted as previously discussed producing Figure 20. From this figure the VSWR was determined to be 5.67 which yielded a reflection coefficient of .70. The distance from the feed aperture to the point of maximum apparent impedance in the line was measured from the plots of Figure 20 at .418 wavelengths. This information when applied to the transmission line Smith Chart as previously described yielded the apparent impedance:

$$Z_a = 32.4 - j78.3 \text{ ohms}$$

or admittance,

$$Y_a = 1/Z_a = 4.51 + j10.9 = 11.8\angle 67.5^\circ \text{ millimhos}$$

By applying the feed point correction for 300 MHz to this value as previously discussed we obtain the measured input admittance adjusted for zero base separation;

$$Y_{om} = 4.51 + j8.73 = 9.83\angle 62.7^\circ \text{ millimhos}$$

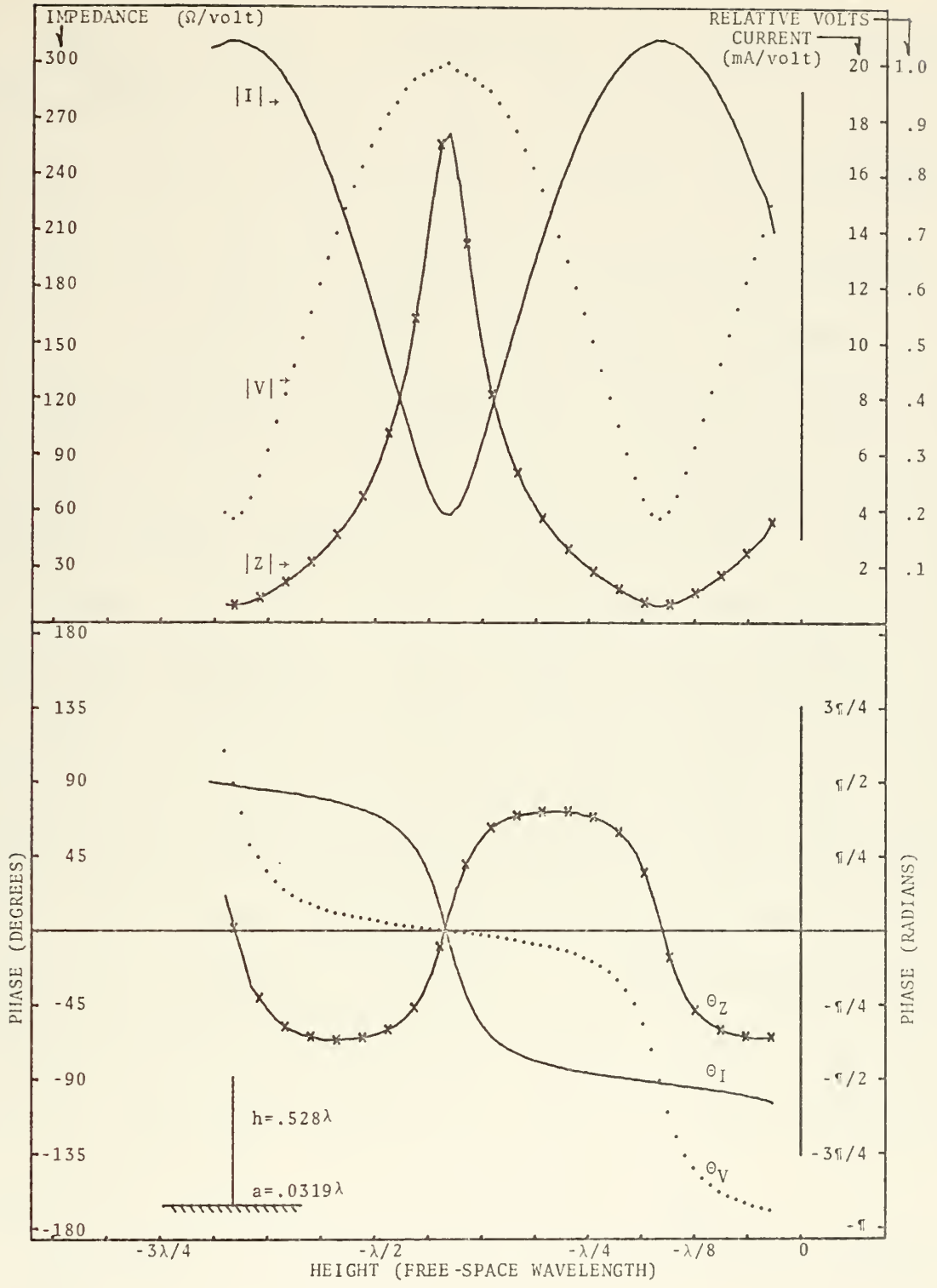

Figure 20. -

Measured current and charge, and calculated impedance (relative to 1 volt at maximum charge) within a coaxial feed system terminated in a .528 wavelength monopole.

Using a linear extrapolation of the tabulated King-Middleton solutions [King 1956, Table 30.3] we find the theoretical value of Y_o for a monopole by multiplying the tabulated value by 2 (dipole to monopole conversion):

$$Y_o = 4.35 + j18.42 = 18.92\angle 76.7^\circ \text{ millimhos}$$

Comparison of the measured and tabulated values of conductance shows a +3.7 percent (referenced to the tabulated value) variation in the measured value. This is considered to be within experimental accuracy. The susceptance variation of -52.6 percent is not considered to be within experimental accuracy; however, comparison of the extrapolated experimental results of Hartig with the second-order theory of King and Middleton [King 1956, Table 38.6] shows similar percentage errors near antiresonance for values of between 7.2 and 7.5. In these comparisons the difference between experiment and theory was 21 percent for location of antiresonance, 9.5 percent for the location of R_{max}, and 37 percent for the magnitude of R_{max}.

The above discussion of susceptance difference actually distorts the significance of this variation. Consideration of the phasor angle of the admittance places this difference in proper perspective. From the King-Middleton tabulated

admittance an angle of 76.7 degrees is predicted for this case. The measured, adjusted admittance angle is 62.7 degrees, while the admittance angle read from the impedance phase plot of Figure 20 (an independent measurement) is 62.8 degrees. The percent variations, referenced to 90 degrees, are -15.6 and -15.4 percent respectively for the adjusted admittance angle and the impedance phase plot angle.

At 195 MHz two monopoles were selected for comparison with tabulated data. The 52.8 cm monopole considered at 300MHz had a $\beta_o h$ of 2.156 at 195 MHz which was within the range of tabulated values for the King-Middleton second-order solutions, and was also used at 195 MHz. For the second comparison an 87 cm monopole was chosen to give $\Omega = 8.00$ and $\beta_o h = 3.5531$ which were also within the range of tabulated values.

Figure 21 shows the data plot within the feed system for the 52.8 cm monopole at 195 MHz. From this figure a VSWR of 3.38 was determined and the impedance maximum was located .49 wavelengths from the feed aperture. The reflection coefficient calculated from this VSWR was .543. From these values the apparent impedance and admittance was found as previously discussed:

$$Z_a = 160.7 - j30.44 \text{ ohms}$$

$$Y_a = 6.01 + j1.14 = 6.12\angle 10.7^\circ \text{ millimhos}$$

Applying the feed point correction to this value yields:

$$Y_{om} = 6.01 - j.27 = 6.02\angle -2.57^\circ \text{ millimhos}$$

The King-Middleton solutions [King 1956, Table 30.11] with a linear extrapolation between tabulated values predicts:

$$Z_o = 168.0 - j5.11 \text{ ohms}$$

or

$$Y_o = 1/Z_o = 5.95 + j.18 = 5.95\angle 1.73^\circ \text{ millimhos}$$

The variation in conductance in this case is +1.0 percent while the variation in admittance phase angle referenced to 90 degrees is -4.8 percent. The admittance phase angle, determined from the impedance phase plot, is -10.1 degrees which is a variation of -13.1 percent from the King-Middleton second-order solution predicted value.

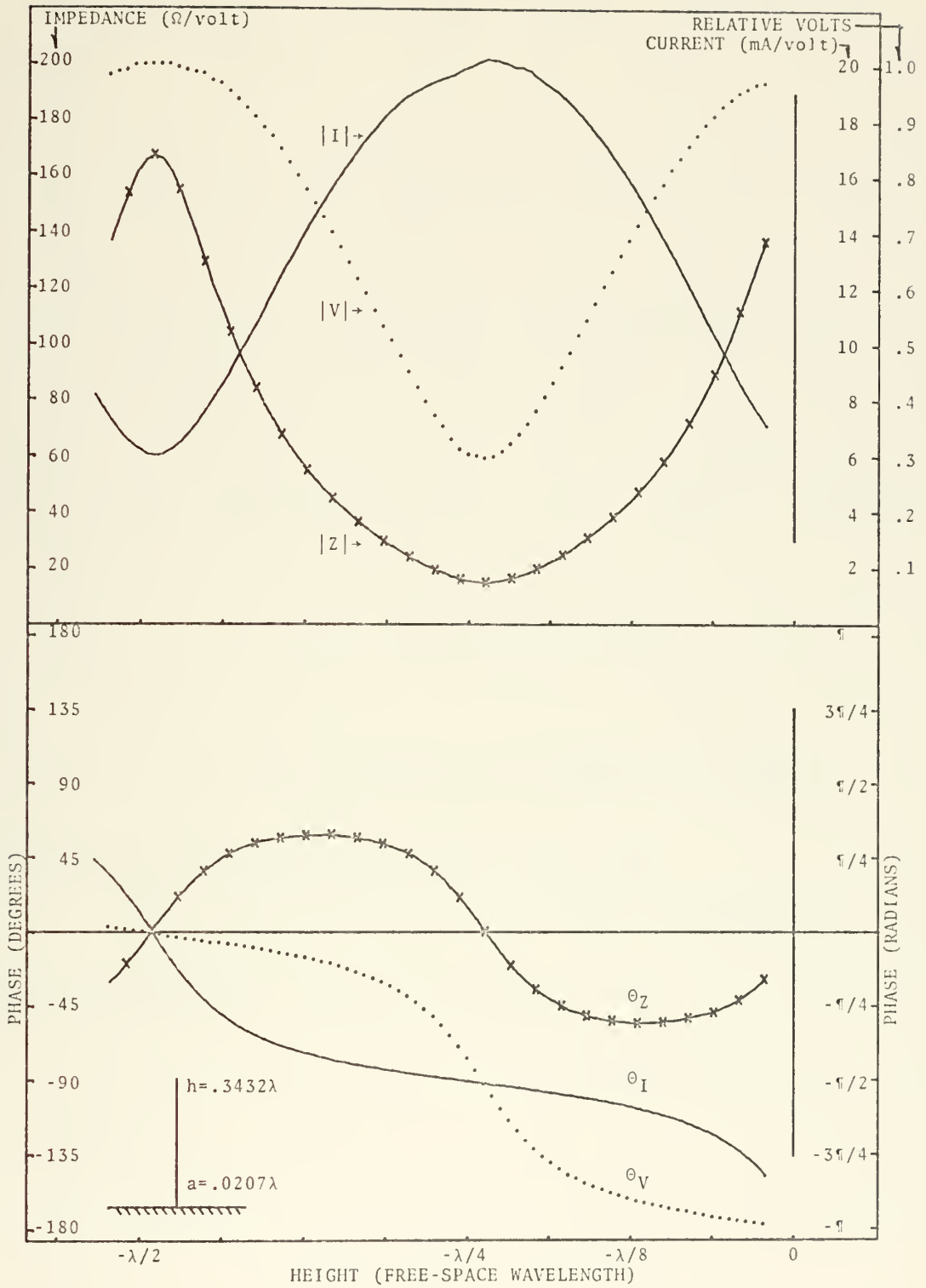

Figure 21. -

Measured current and charge, and calculated impedance (relative to 1 volt at maximum charge) within a coaxial feed system terminated in a .3432 wavelength monopole.

The data plot of charge and current distributions and calculated impedance within the coaxial feed system terminated in an 87 cm monopole driven at 195 MHz is shown in Figure 22. The VSWR was found to be 6.39 from Figure 22. The distance fron the maximum apparent impedance to the antenna/image plane interface, also determined from Figure 22, was measured as .4205 wavelengths. The above VSWR yielded a reflection coefficient of .729. Transmission line Smith Chart calculations using the above information yielded:

$$Z_a = 32.44 - j81.34 \text{ ohms}$$

and

$$Y_a = 4.23 + j10.6 = 11.4 \angle 68.2^\circ \text{ millimhos}$$

With the terminal-zone correction we find:

$$Y_{om} = 4.23 + j9.19 = 10.1 \angle 65.3^\circ \text{ millimhos}$$

The King-Middleton solution predicts:

$$Y_o = 4.505 + j13.19 = 13.94 \angle 71.1^\circ \text{ millimhos}$$

for this case.

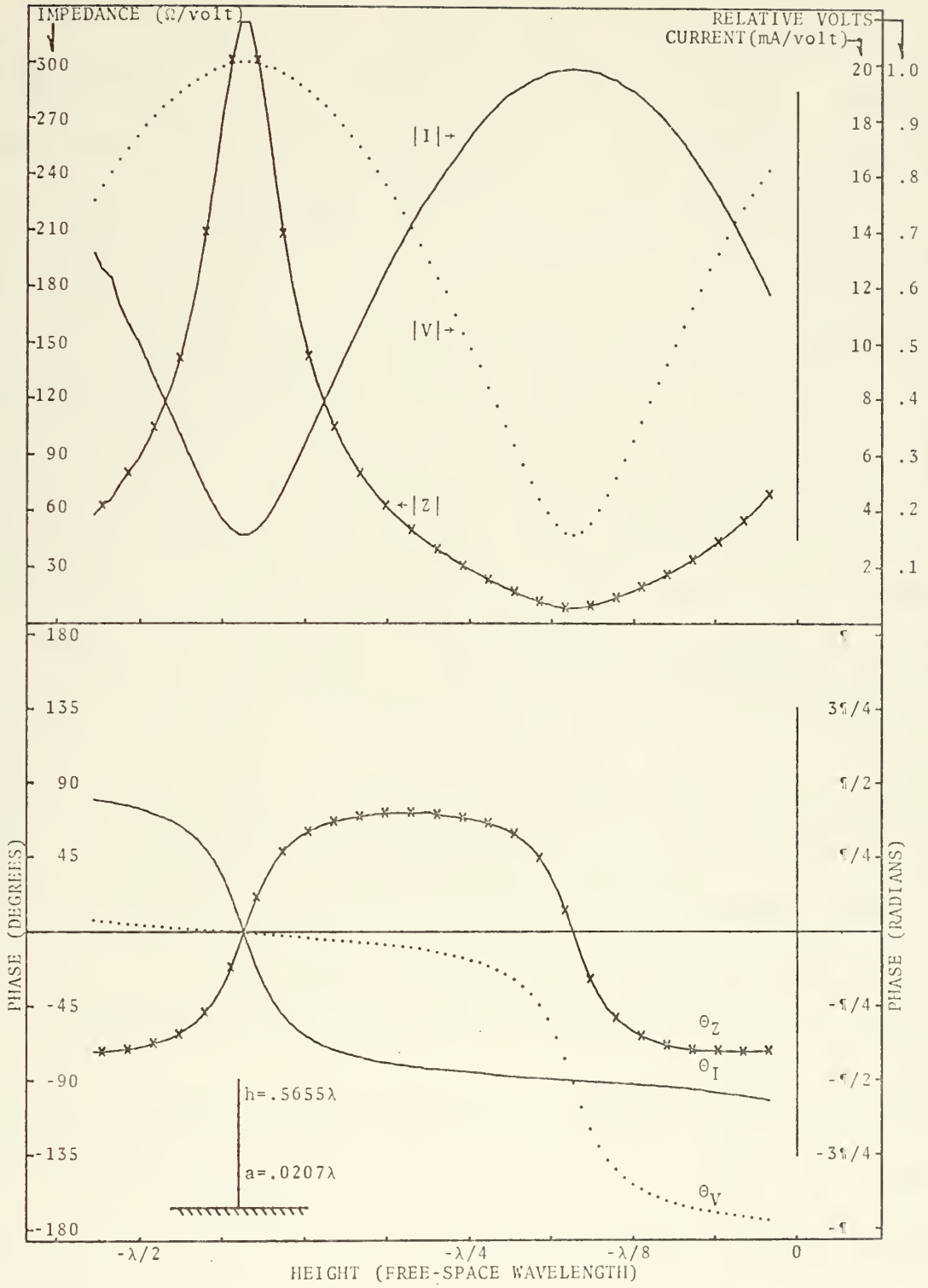

Figure 22. -

Measured current and charge, and calculated impedance (relative to 1 volt at maximum charge) within a coaxial feed system terminated in a .5655 wavelength monopole.

Variations in this case were -6.1 percent for conductance, -6.4 percent for the measured adjusted admittance angle, and no variation for the phase angle of 71.1 degrees determined from the impedance phase plot.

Although the 3 cases of comparison of experimental results obtained herein with the King-Middleton second-order solutions for monopole impedance are far from exhaustive, they demonstrate that the measurement technique applied in this work produces results which are consistent with the theory and previous experimental work. Conductance, which (as previously discussed) is essentially independent of feed aperture dimensions, has been found to be within 6.1 percent of that predicted by the theory. The admittance phasor angle was consistently measured less than that predicted by the King-Middleton second-order theory; 15.6 percent less at 300 MHz, and, in the worst case, 6.4 percent less at 195 MHz. Considering that small base separation ($\beta_o (b - a)$ much less than 1) was assumed for lumped element treatment of the feed aperture correction [King 1956, p. 149], and that $\beta_o (b - a)$ was .46 and .30 at 300 and 195 MHz respectively; the degree of correlation between predicted and experimental admittance angles is considered good.

b. Reference Monopoles

As previously discussed, a reference monopole was chosen such that its physical height was equal to that of the crossed-monopole. Figures 23 and 24 show the measured charge and current distributions and the impedance calculated from these distributions within a feed system terminated in a 136.8 cm monopole excited at 300 and 195 MHz respectively.

From Figure 23, using the procedure previously detailed, the apparent impedance of the 136.8 cm monopole excited at 300 MHz (1.368 wavelength monopole) was determined.

$$Z_a = 93.8 - j67.9 \text{ ohms}$$

and

$$Y_a = 1/Z_a = 7.00 + j5.07 = 8.64\angle 35.9^\circ \text{ millimhos}$$

The admittance phasor angle read from the impedance phase plot of Figure 23 was 37.2 degrees, which is in excellent agreement with that determined by the voltage standing-wave ratio method from the charge magnitude plot.

At 195 MHz the impedance of the 136.8 cm (.8892 wavelength) monopole was determined from Figure 24.

$$Z_a = 113.3 - j95.8 \text{ ohms}$$

and

$$Y_a = 1Z_a = 5.15 + j4.35 = 6.74\angle 40.2^\circ \text{ millimhos}$$

The admittance phasor angle determined from the impedance phase plot (38.8 degrees) is again in excellent agreement with that determined from the magnitude plot.

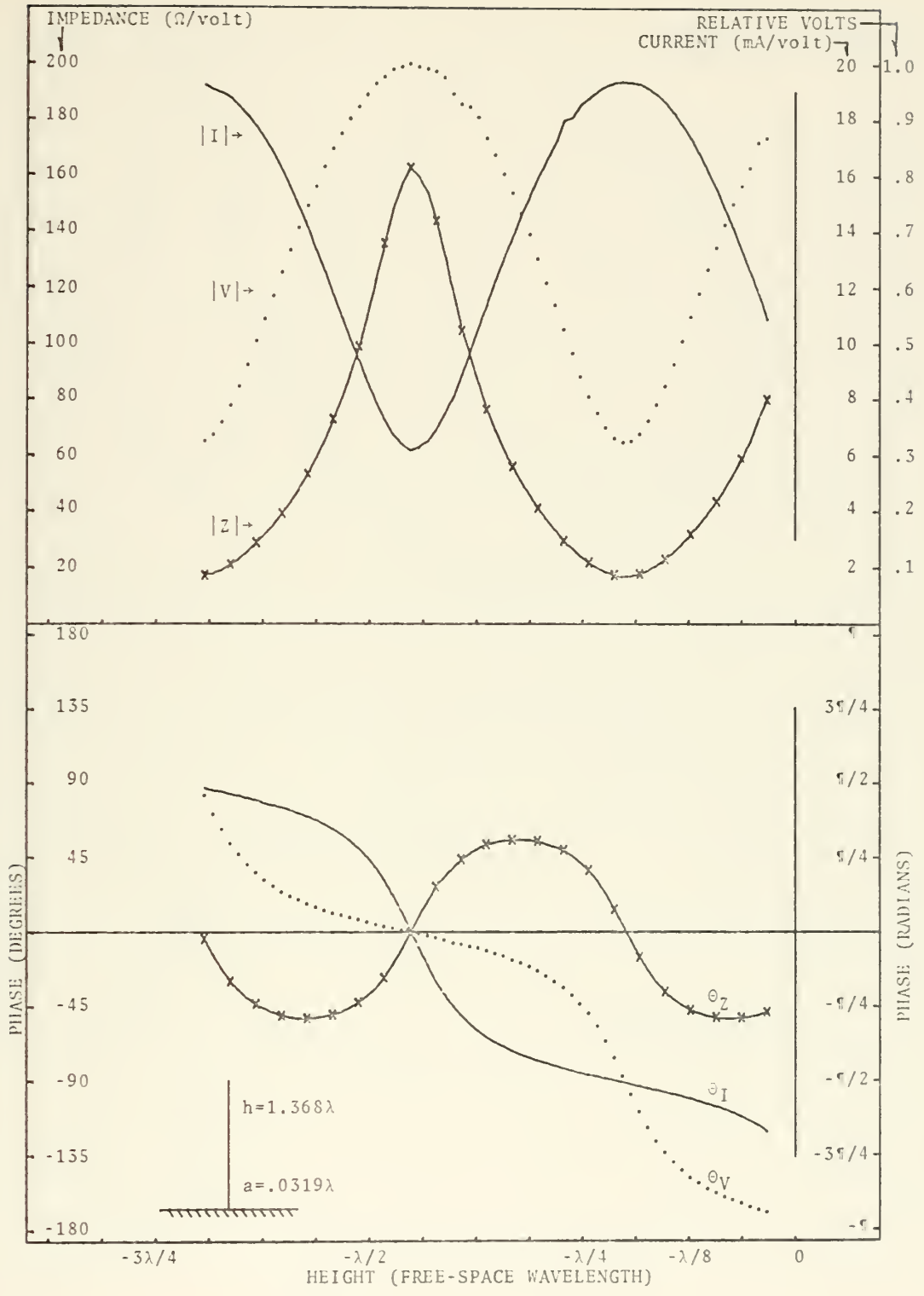

Figure 23. -

Measured current and charge, and calculated impedance (relative to 1 volt at maximum charge) within a coaxial feed system terminated in a 1.368 wavelength monopole.

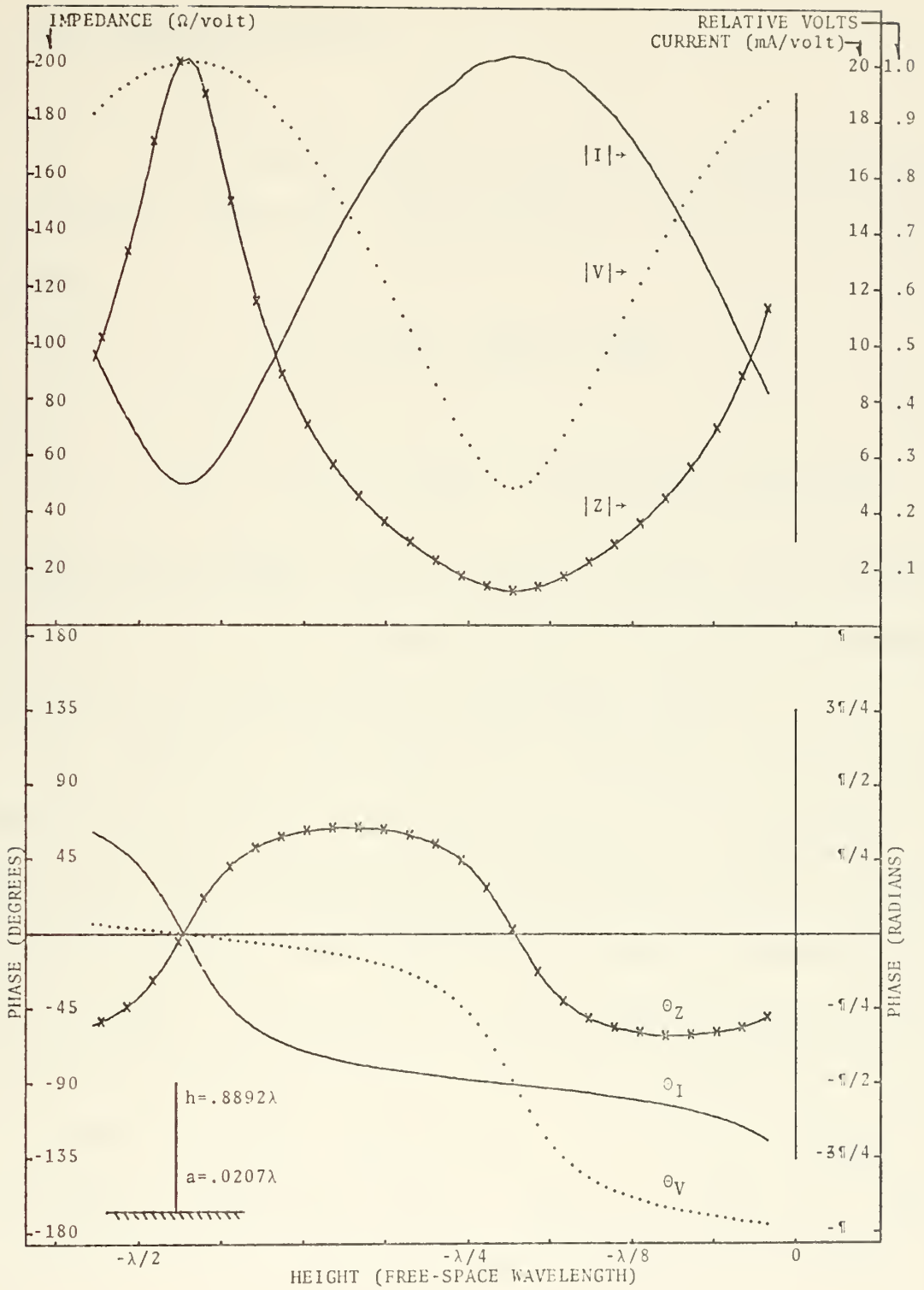

Figure 24. -

Measured current and charge, and calculated impedance (relative to 1 volt at maximum charge) within a coaxial feed system terminated in a .8892 wavelength monopole.

4. Crossed-Monopoles

a. CASE 1

Feed system plots of the CASE 1 crossed-monopole are shown in Figure 25. The technique previously described yielded:

$$Z_a = 90.3 - j88.3 \text{ ohms}$$

and

$$Y_a = 1/Z_a = 5.66 + j5.53 = 7.91\angle 44.3^\circ \text{ millimhos}$$

The admittance phasor angle measured from the impedance phase plot was 44.2 degrees, again in excellent agreement with that determined from the magnitude plots.

As previously discussed, the addition of horizontal "loading" arms on the reference monopole is expected to effectively add capacitance in parallel with the antenna. The decrease in the real part of the apparent impedance and the increase in the admittance phase angle as compared with that of the reference monopole are both manifestations of the added parallel capacitance. The total change in admittance is relatively small. This, as will be later seen, is related to the minor disturbance of the charge and current distributions of the vertical member by the addition of horizontal elements in this configuration.

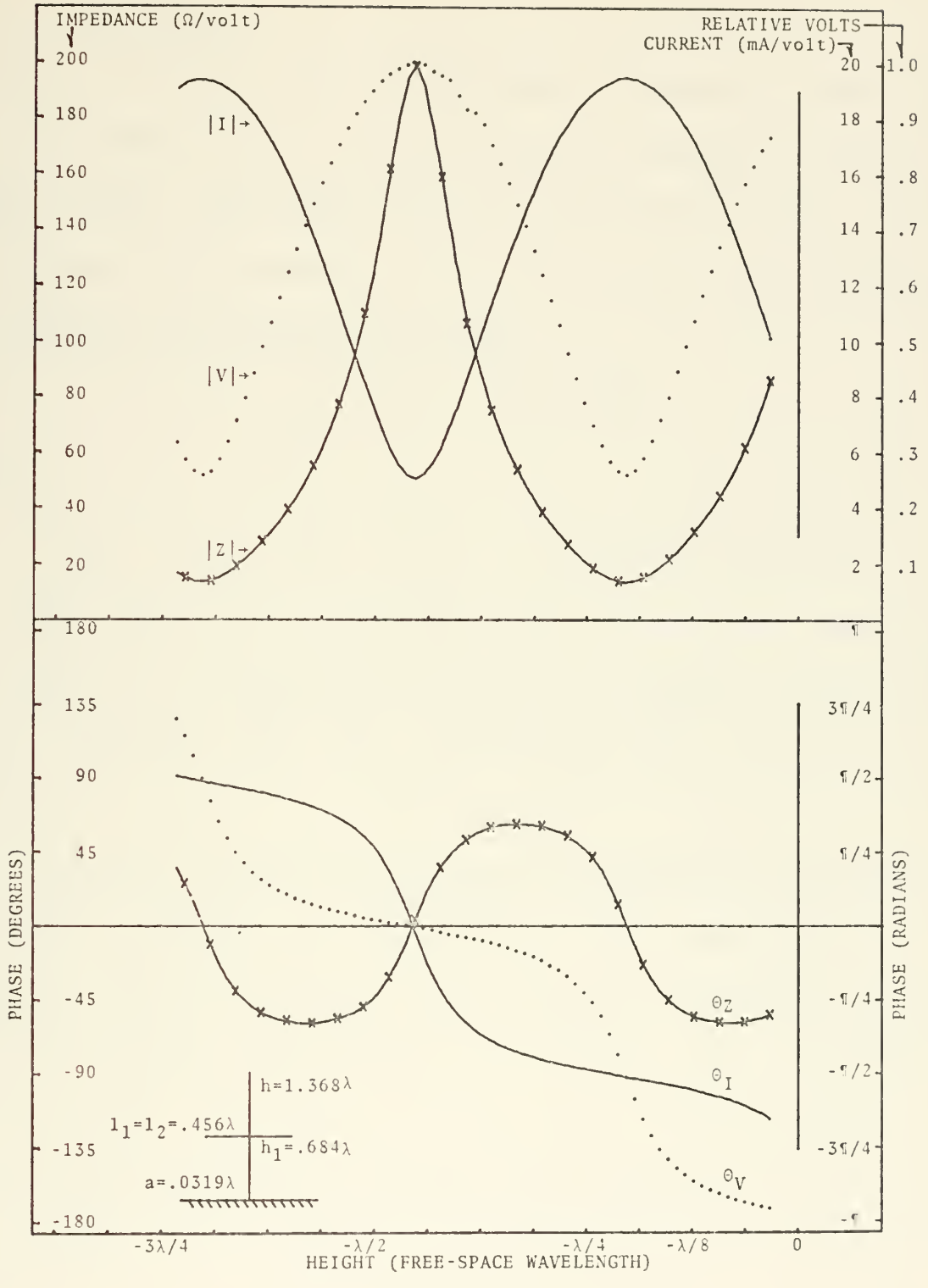

Figure 25. -

Measured current and charge, and calculated impedance (relative to 1 volt at maximum charge) within a coaxial feed system terminated in a CASE 1 crossed-monopole.

b. CASE 2

Figure 26 is the graph of measured charge and current distributions and the calculated impedance within a feed system terminated in a CASE 2 crossed-monopole. From this graph the impedance at the feed point aperture was determined as previously discussed:

$$Z_a = 89.3 - j58.9 \text{ ohms}$$

and

$$Y_a = 1/Z_a = 7.80 + j5.15 = 9.35\angle 33.4^\circ \text{ millimhos}$$

In this case the admittance angle determined from the plotted curve of impedance phase is 34.1 degrees, again in good agreement with that determined from the magnitude plots.

We again expect the addition of horizontal arms to the reference monopole to effectively add capacitance in parallel with the antenna with a resultant decrease in the real part of the impedance and an increase in the phasor angle of the admittance. The real part of the impedance is seen to decrease from 98.3 ohms in the reference monopole to 89.3 ohms in the CASE 2 crossed-monopole; however, the measured 33.4 degree admittance phase of this crossed-monopole configuration indicates a 2.5 degree decrease from that of the reference monopole. This

discrepancy is not considered within the accuracy of the experimental results achieved herein. A later discussion of the charge and current distributions on the vertical member of this case crossed-monopole will show minimal disturbance of these distributions from those of the reference monopole, which is consistent with the magnitude of change of the admittance phase.

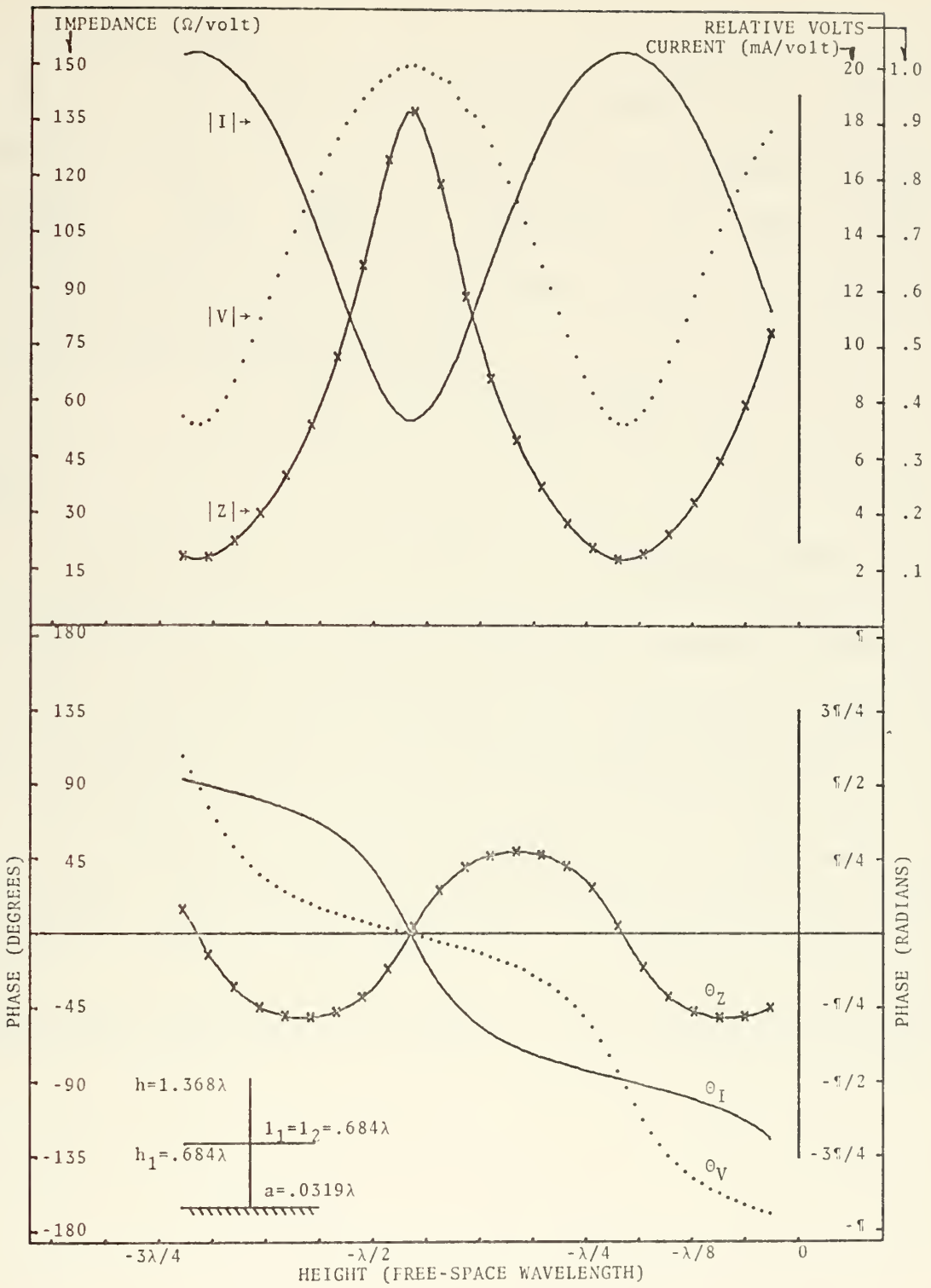

Figure 26. -
Measured current and charge, and calculated impedance (relative to 1 volt at maximum charge) within a coaxial feed system terminated in a CASE 2 crossed-monopole.

c. CASE 3

In this case horizontal, antiresonant arms were added at a point of charge maximum on the reference vertical monopole. The apparent impedance of the CASE 3 crossed-monopole was determined from Figure 27 with the technique previously described.

$$Z_a = 21.8 - j21.8 \text{ ohms}$$

and

$$Y_a = 1/Z_a = 22.9 + j22.9 = 32.4\angle 45^\circ \text{ millimhos}$$

The admittance angle measured from the impedance phase plot was 44.5 degrees, which supports that calculated from the charge magnitude plot by the standing-wave ratio method.

The parallel capacitance view of the addition of horizontal "loading" arms is suported in this case by the decrease in the real part of Z_a and the increase in admittance phase with comparison to the reference monopole.

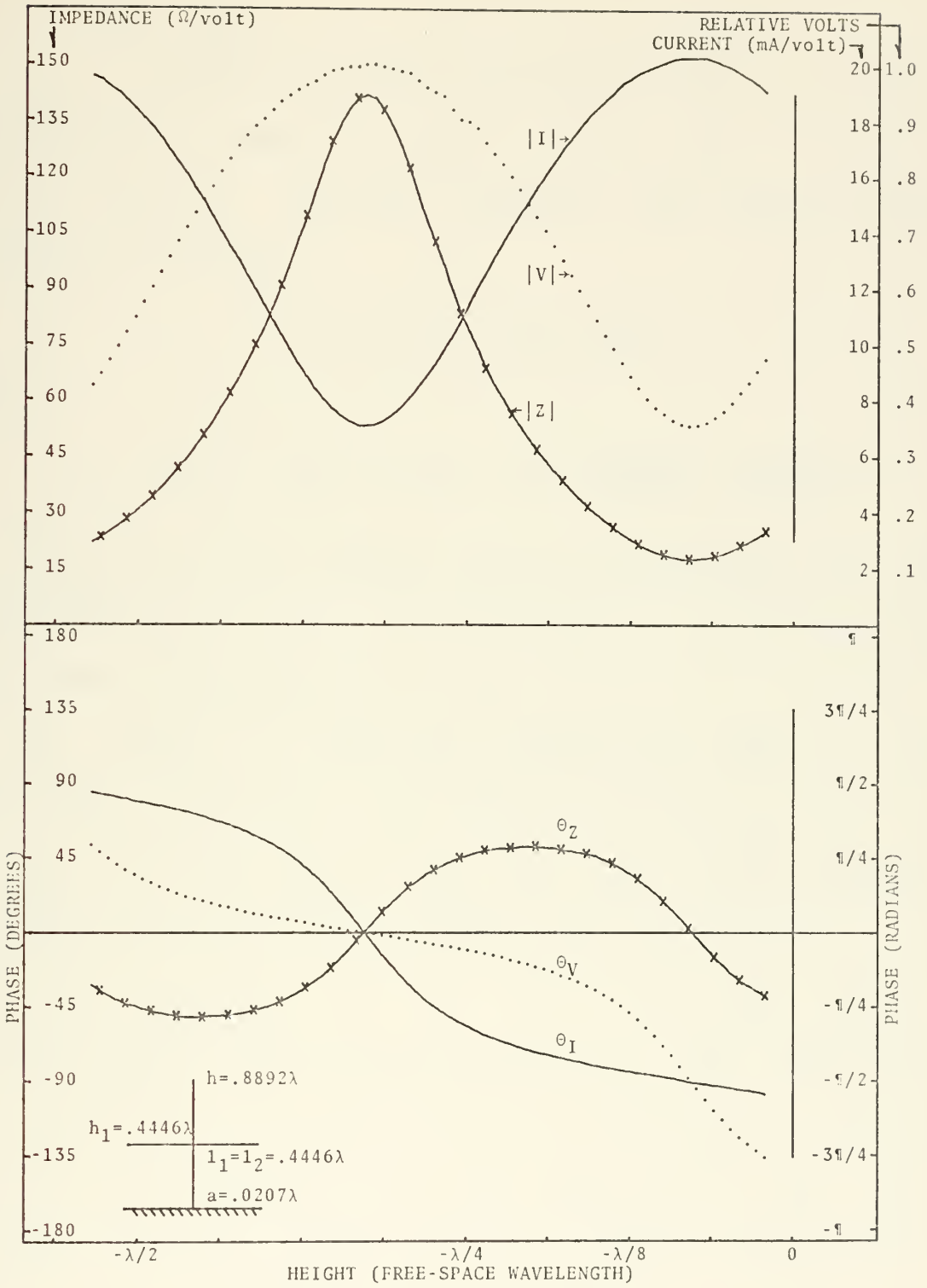

Figure 27. -

Measured current and charge, and calculated impedance (relative to 1 volt at maximum charge) within a coaxial feed system terminated in a CASE 3 crossed-monopole.

d. CASE 4

Figure 28 shows the measured charge and current distributions within the feed system of a CASE 4 crossed-monopole. Apparent impedance and admittance were determined yielding:

$$Z_a = 7.9 - j75.8 \text{ ohms}$$

and

$$Y_a = 1/Z_a = 1.36 + j13.0 = 13.1\angle 84.0^\circ \text{ millimhos}$$

The admittance angle measured one-half wavelength from the feed aperture in Figure 28 was 83 degrees; in good agreement with that determined above.

The effect of parallel capacitance added to the reference monopole by the resonant horizontal arms is dramatic in this case. The real part of the apparent impedance is seen to have decreased from 113.3 ohms in the reference monopole to 7.9 ohms for the CASE 4 crossed-monopole, while the phase angle of the admittance has increased from 40.2 degrees to 84.0 degrees. In this case the impedance seen at the feed aperture is that of a monopole slightly shorter than a resonant length. This condition can be thought of as resulting from the effects of the antiresonant reference monopole, the feed aperture capacitance, and the capacitance added by the horizontal

arms. The charge and current distributions of this configuration to be discussed in a later section will show the effect of this resonance at the feed aperture.

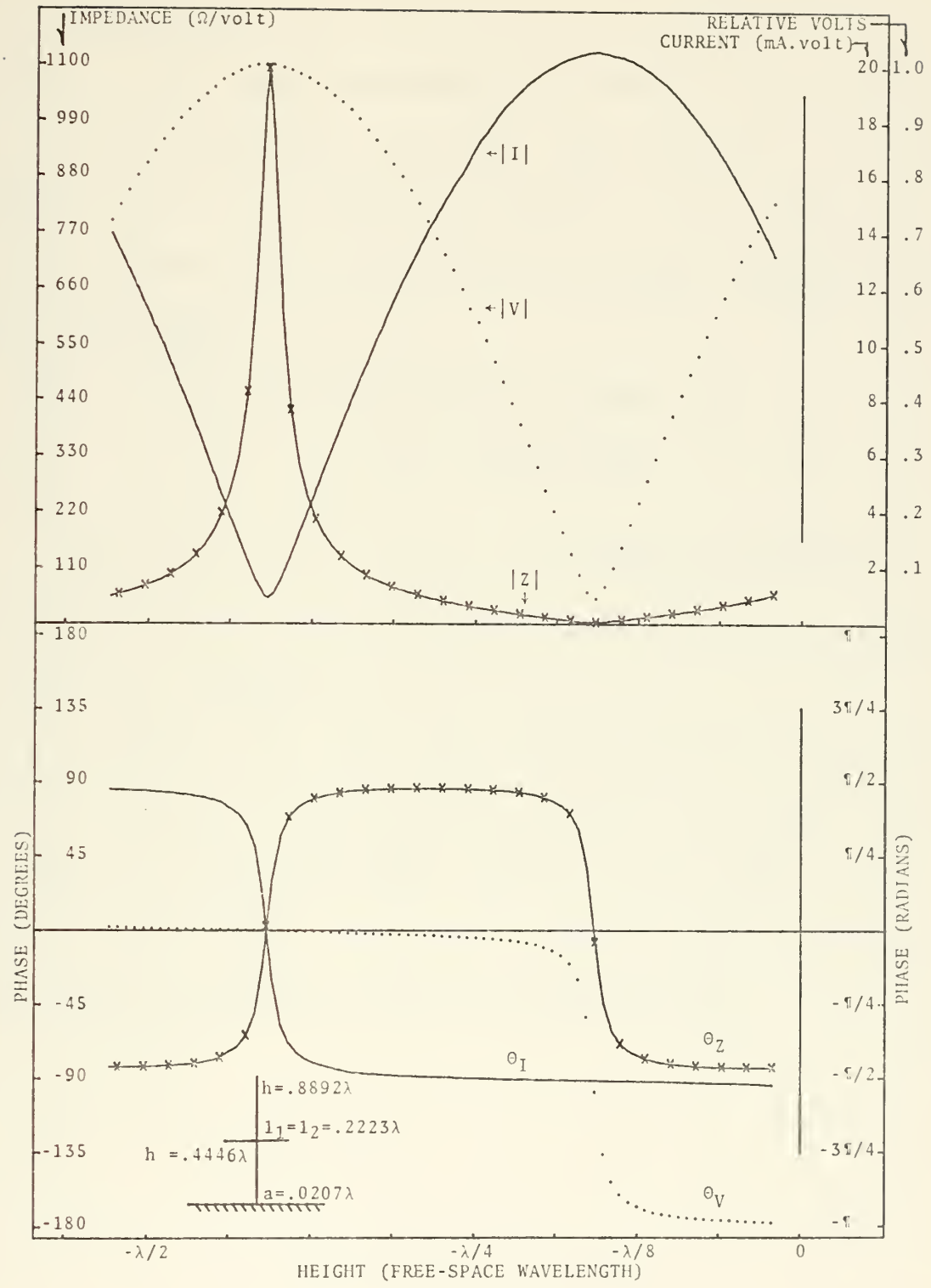

Figure 28. -

Measured current and charge, and calculated impedance (relative to 1 volt at maximum charge) within a coaxial feed system terminated in a CASE 4 crossed-monopole.

e. CASE 5

The CASE 5 configuration resulted from combining one arm from CASE 3 with one arm from CASE 4. It was expected that the observed impedance would combine the effects of each and appear between the values obtained for CASE 3 and CASE 4.

From the data plots presented in Figure 29:

$$Z_a = 16.5 - j66.4 \text{ ohms},$$

$$Y_a = 1/Z_a = 3.53 + j14.2 = 14.6\angle 76.0^\circ \text{ millimhos},$$

and the admittance angle determined from the impedance phase plot was 76.7 degrees.

As expected the real part of the impedance decreased from the reference value more than in CASE 3, but less than in CASE 4. The admittance angle in this case was also between the values obtained in CASE 3 and 4 further supporting the parallel capacitive loading view.

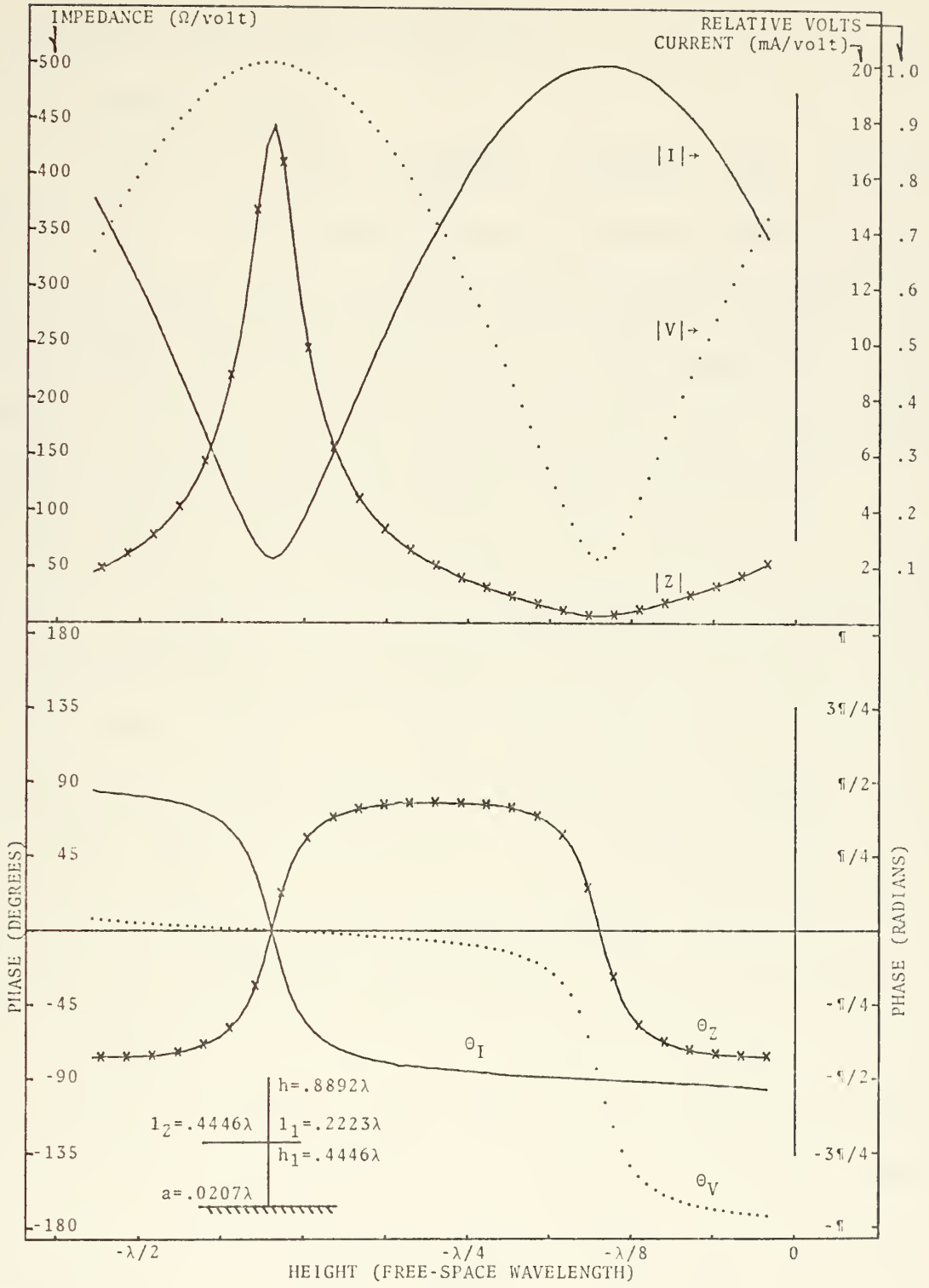

Figure 29. -

Measured current and charge, and calculated impedance (relative to 1 volt at maximum charge) within a coaxial feed system terminated in a CASE 5 crossed-monopole.

C. CHARGE AND CURRENT DISTRIBUTIONS

1. Display Format

Graphs of the measured charge and current distributions on the transmitting crossed-monopole antennas are divided into upper and lower parts as were those of the distributions within the feed system. The upper part shows measured charge and current magnitude while the lower part presents measured relative phase of these quantities.

The graphs are also divided into left and right sections. Charge and current measurements taken from the horizontal data arm are plotted in the right sections where the abscissa, common to the upper and lower parts, is labeled "X". The X-axis, as defined in Figure 18, originates at the center of the vertical member and dimensions the data arm. Distance along the X-axis is indicated in free-space wavelength. Vertical charge and current measurements are shown in the left sections of the graph where the abscissa, also common to the upper and lower parts, is labeled Z indicating the Z-axis. The Z-axis (see Figure 18) originates at the antenna/Image plane interface and dimensions the vertical element. Distance along the Z-axis is also indicated in free-space wavelength.

Crossed-Monopole charge and current magnitudes for both

the vertical and the horizontal arm distributions are labeled $|\rho|$ and $|I|$ respectively. Phase of these quantities is indicated by θ and θ_I. Also shown in the left section of the graph are the charge and current distributions of the reference monopole which have which have been distinguished by the addition of an X indicating the approximate position of every third data point on the curves, and by the addition of the subscript R to the appropriate curve labels.

The vertical dashed line which is located in the approximate center of the left section indicates the point of attachment of the horizontal arms to the vertical monopole.

2. Crossed-Monopoles

a. CASE 1

Measured charge and current distributions in the vicintiy of the junction of the CASE 1 crossed-monopole and its reference monopole are shown in Figure 30. Consideration of the charge and current distributions present on the reference monopole shows the arms to have been positioned at a point of maximum current/minimum charge as was desired for this case. The charge and current distributions on the antiresonant arms are seen to be approximated by the zero-order antiresonant response as

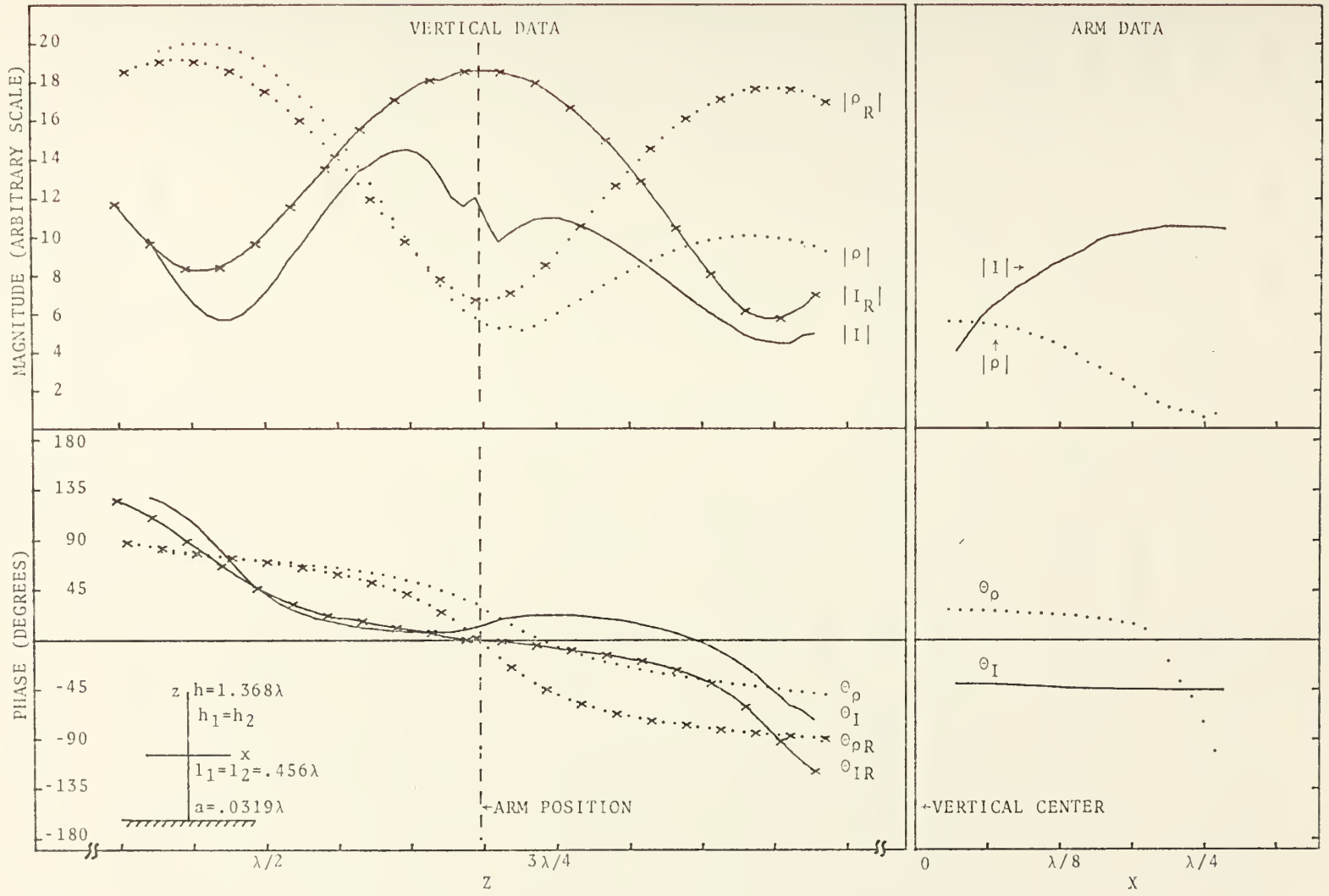

Figure 30. - Measured charge and current on a transmitting monopole and crossed-monopole. Junction at maximum current minimum charge.

predicted for excitation of the horizontal arms by junction charge (see Figure 3.a.). Charge distribution on the arm is seen to converge to the value of the charge distribution on the vertical element in both magnitude and phase as the junction is approached. The vector sum of the currents entering the junction can also be seen to be zero as expected.

Disturbance of the charge and current distributions on the vertical element from those of the reference monopole can be seen to be relatively minor below the junction. Above the junction the distributions have nearly the same locations of maxima and minima as those of the reference monopole, but the magnitudes are reduced. These distributions on the upper extension of the vertical element above the junction are seen to be approximated by the zero-order resonant response depicted in Figure 1.a. with non-zero minimums. The extension of the vertical element above the junction can be viewed as both voltage and current fed; that is, excited by the junction charge and the self inductance of the vertical member at the junction with the currents flowing on the horizontal arms reducing the coupling to the upper vertical element.

Locations of maximum current/minimum charge and vice versa on the vertical element, as indicated by points on the

vertical phase plot where charge and current are in phase, can be seen to be shifted slightly away from the feed point as compared with those of the reference monopole. This is consistent with the slight apparent lengthening of the antenna, compared with the reference monopole, observed in the impedance measurements.

The irregularity in the vertical element current distribution plot at the point of attachment of the arms resulted from slight dislocation of the probe as it passed over the junction of the vertical and horizontal surface slots and is not considered significant.

b. CASE 2

Figure 31 shows the measured charge and current distributions on a CASE 2 crossed-monopole in the vicinity of the junction. Consideration of the reference monopole distributions, also shown in Figure 31, again shows the horizontal arms to be positioned at a current maximum/charge minimum on the reference monopole. At the junction charge magnitude and phase measured on the arms was equal to that measured on the vertical member. Kirchoff's Current Law can also be seen to be obeyed by vector addition of the currents in each element near the junction.

Disturbance of the vertical charge and current distributions by the addition of three-quarter wavelength

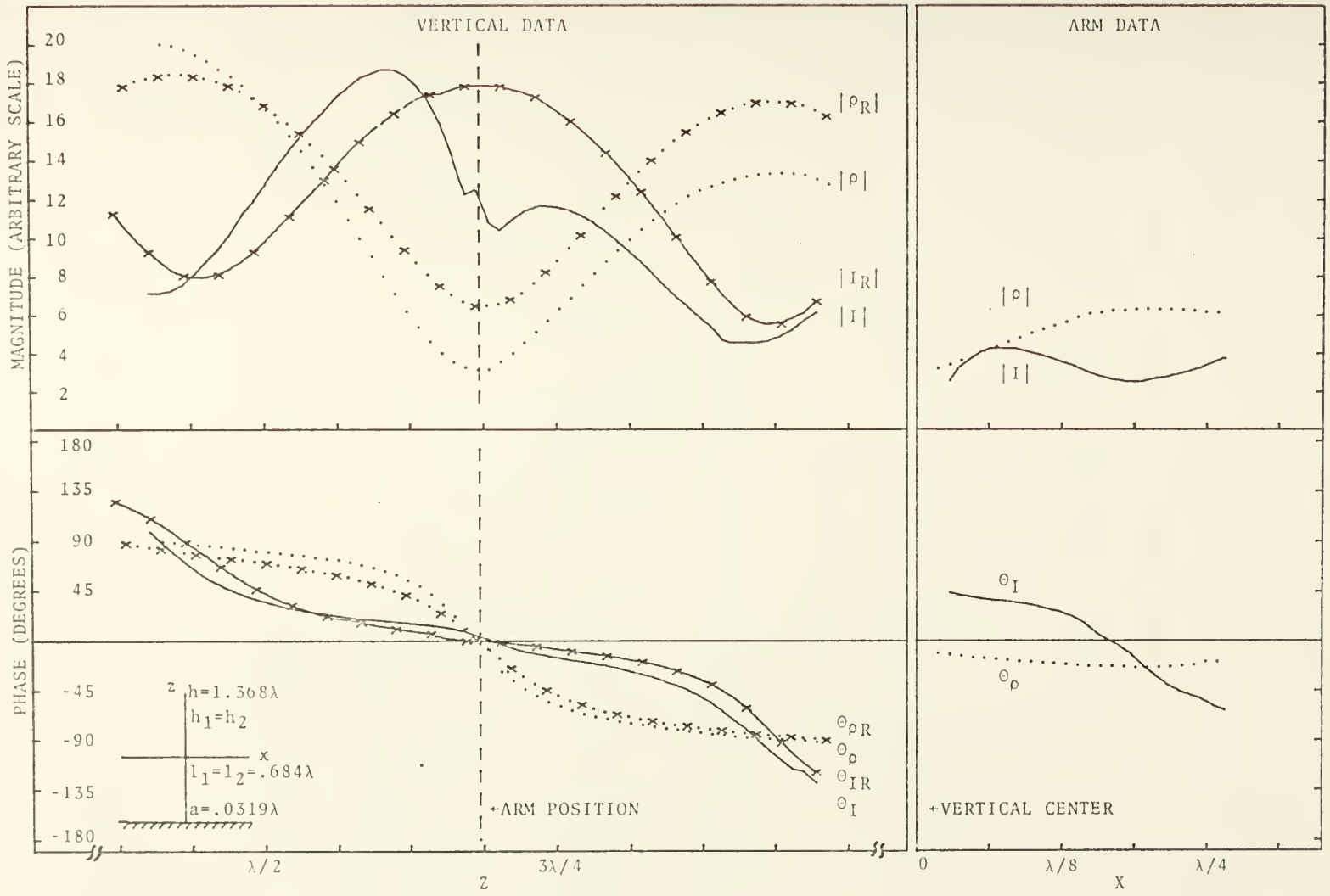

Figure 31. - Measured charges and currents on a transmitting monopole and crossed-monopole. Junction at maximum current minimum charge.

resonant horizontal arms is minimal both above and below the junction in this case. The small currents on the arms which result from junction charge excitation of the resonant arms are a combination of the resonant and antiresonant responses of these arms. Since the currents on the arms are relatively small the inductive coupling to the upper resonant extension of the vertical element above the junction is little diminished from that of the reference monopole. The response in this upper element is again approximated by the resonant response of Figure 1.a. with non-zero minimums.

Locations of charge maxima/current minima and vice versa along the vertical element when compared with those of the reference monopole can be seen to be slightly shifted toward the feed point. This is most easily seen by consideration of the points where charge and current are in phase. This slight shift of the standing-wave distributions toward the feed point signifies an apparent shortening of the antenna when viewed from the antenna/image plane interface. This was also observed in the impedance measurement for this case antenna; however, the 2.5 degree decrease in the admittance phasor angle was so slight as not to be considered within experimental accuracy. Consideration of the charge distribution on the horizontal arms offers a possible

explanation for the apparent shortening of the antenna by the addition of these arms. From the arm data plot of Figure 31 the charge distribution can be seen to be approaching a maximum one-quarter wavelength from the vertical member. This distribution is constrained by boundary conditions to be a maximum at the end of the arm three-quarter wavelengths from the vertical member. A summation of the capacitive effects resulting from this charge distribution along the horizontal arm, when transformed to the vertical member by a transmission line analogy, might result in an apparent inductive reactance in parallel with the antenna, making it appear shortened.

c. CASE 3

The CASE 3 crossed-monopole measured charge and current distributions with those of the reference monopole are shown in Figure 32. In this case the point of attachment of the horizontal arms can be seen to be at maximum charge/minimum current on the reference monopole. The general distributions of charge and current on the vertical element have been seriously disturbed from those of the reference monopole by the addition of antiresonant horizontal arms to the reference monopole at the point of charge maximum. Both Kirchoff's Current Law and continuity of charge can be observed at the junction.

The charge and current distributions on the horizontal arms are approximated by the zero-order antiresonant response resulting from junction charge excitation of the arms as predicted (see Figure 3.a.). The antiresonant length upper section of the vertical element has a charge distribution which is approximated by the zero-order antirescnant response; however, the current distribution is more corplex consisting of a combination of antiresonant and resonant responses in which the junction charge may be viewed as driving the antiresonant response and the self inductance of the vertical member driving the resonant response.

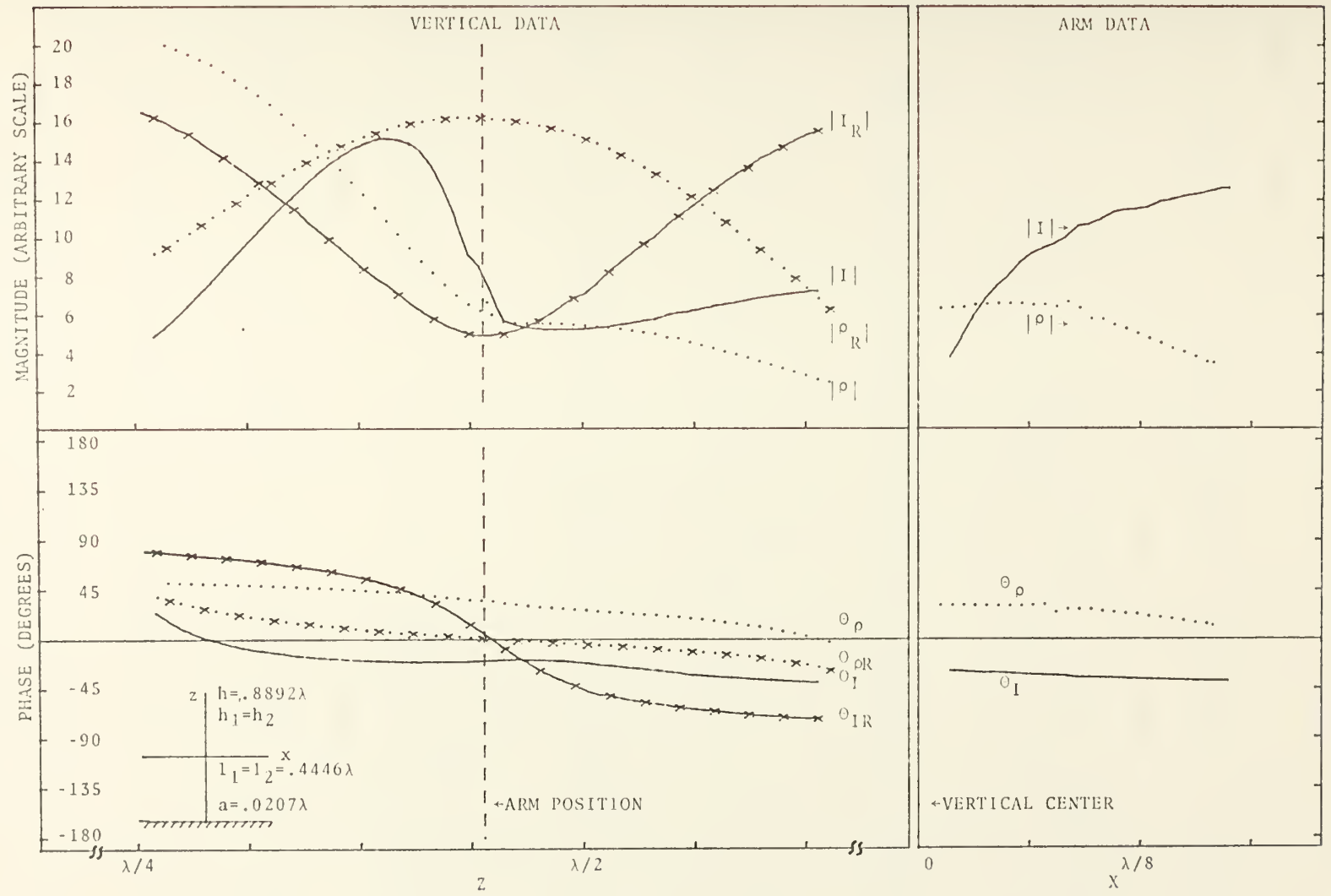

Figure 32. - Measured charges and currents on a transmitting monopole and crossed-monopole. Junction at maximum charge minimum current.

d. CASE 4

Measured charge and current distributions on the CASE 4 crossed-monopole and the reference monopole are shown in Figure 33. Charge magnitude and phase on the data arm are seen to be equal to the respective quantities on the vertical element at the junction. The vector sum of currents entering the junction is also seen to be zero satisfying Kirchoff's Current Law.

The dramatic change in impedance observed in this case is also obvious in the general shape of the charge and current distributions of the lower section of the vertical element. The charge maximum at the position of attachment of the horizontal resonant arms on the reference monopole is seen to have changed to a charge minimum slightly closer to the feed point after attachment of the arms. Assuming an approximate TEM distribution of fields in the vicinity of the lower portion of the vertical element an approximate charge minimum would occur at the feed aperture. This supports the previous observation, made from the impedance measurements for this case, that this antenna was seen as a monopole slightly shorter than resonant length at the feed point.

The measured charge and current distributions on the horizontal arms in this case are essentially those of the

zero-order resonant response shown in Figure 3.b. with an antiresonant response stimulated by the non-zero charge at the junction. The large currents flowing on the horizontal arms limit the effect of the self inductive coupling from the lower to the upper portion of the vertical element and the dislocation of the charge maximum from the junction to the arm extremities reduces the junction charge excitation of this member. The resulting phenomena is a small, nearly antiresonant, response in the antiresonant length segment of the vertical member above the junction.

Horizontal one-quarter wavelength arms located on an antiresonant vertical monopole at the point of charge maximum dominate the antenna transforming the impedance at the feed aperture to that of a resonant monopole.

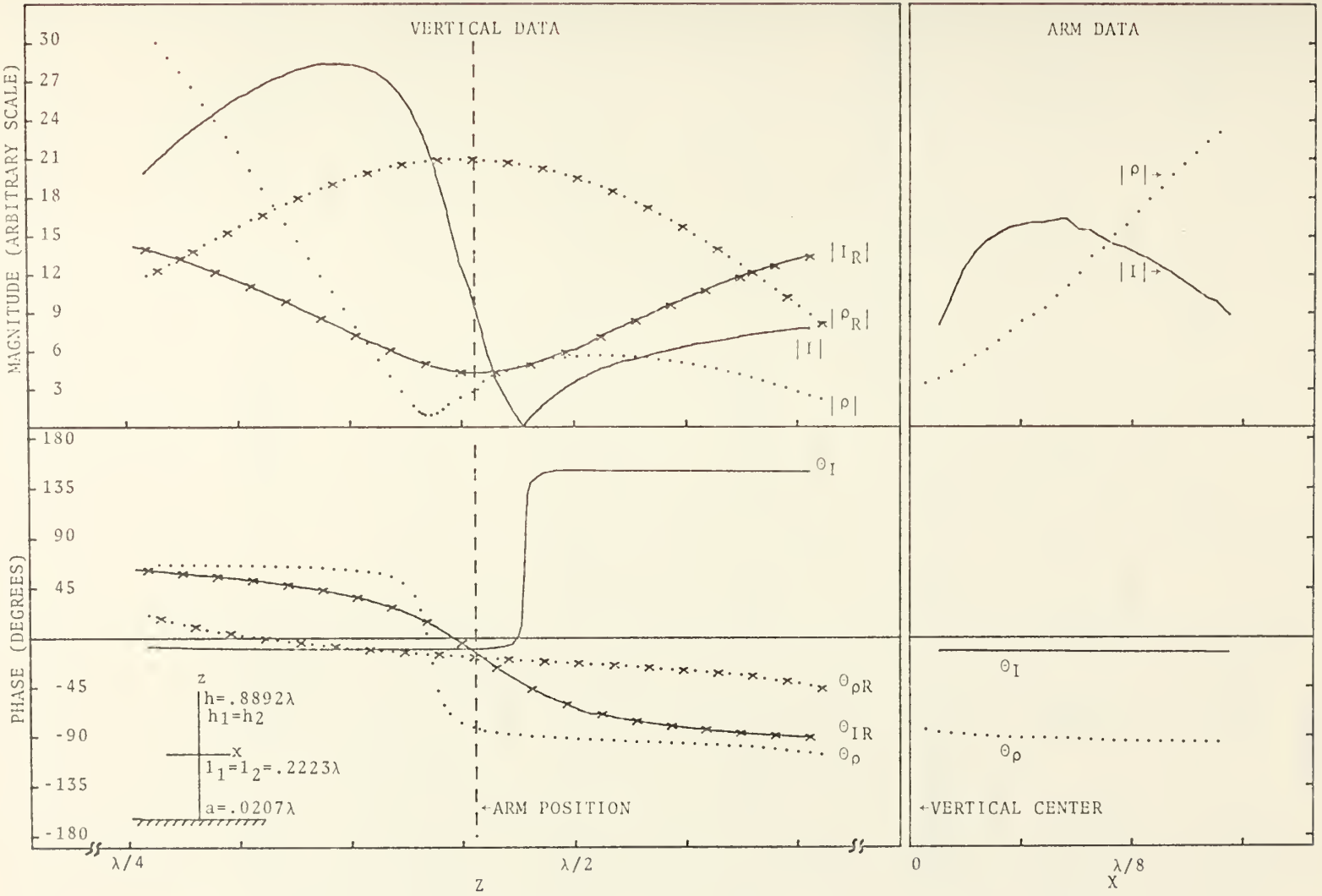

Figure 33. - Measured charges and currents on a transmitting monopole and crossed-monopole. Junction at maximum charge minimum current.

e. CASE 5

The CASE 5 measured charge and current distributions and those of the reference monopole are presented in Figure 34 and 35. In these two figures the reference monopole and vertical surface slot plots of the crossed-monopole are from the same data. The measured charge and current distributions on the resonant arm are shown in Figure 34 and the data from the antiresonant arm is presented in Figure 35.

In the impedance measurement for this case it was observed that the impedance was between the values obtained for CASE 3 and CASE 4. It was also anticipated that the charge and current distributions would show the effects of both arms and be between the extremes of values obtained for CASES 3 and 4. The dominance of the resonant arm was not anticipated, but is clearly evident in the large current and charge distributions on that element and the correspondingly reduced distributions on the antiresonant arm and the antiresonant upper extension of the vertical member above the junction.

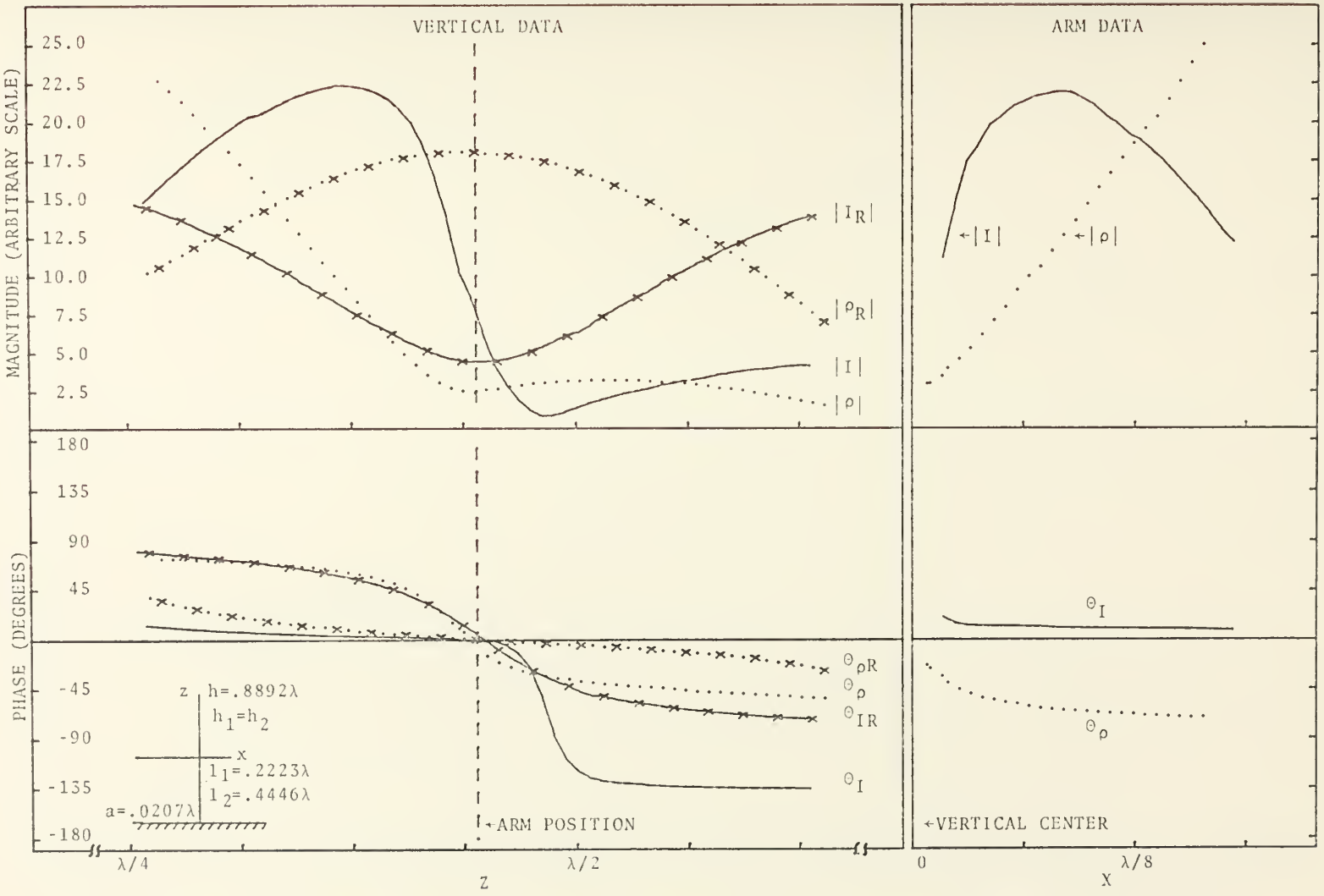

Figure 34. - Measured charges and currents on a transmitting monopole and crossed-monopole. Junction at maximum charge minimum current.

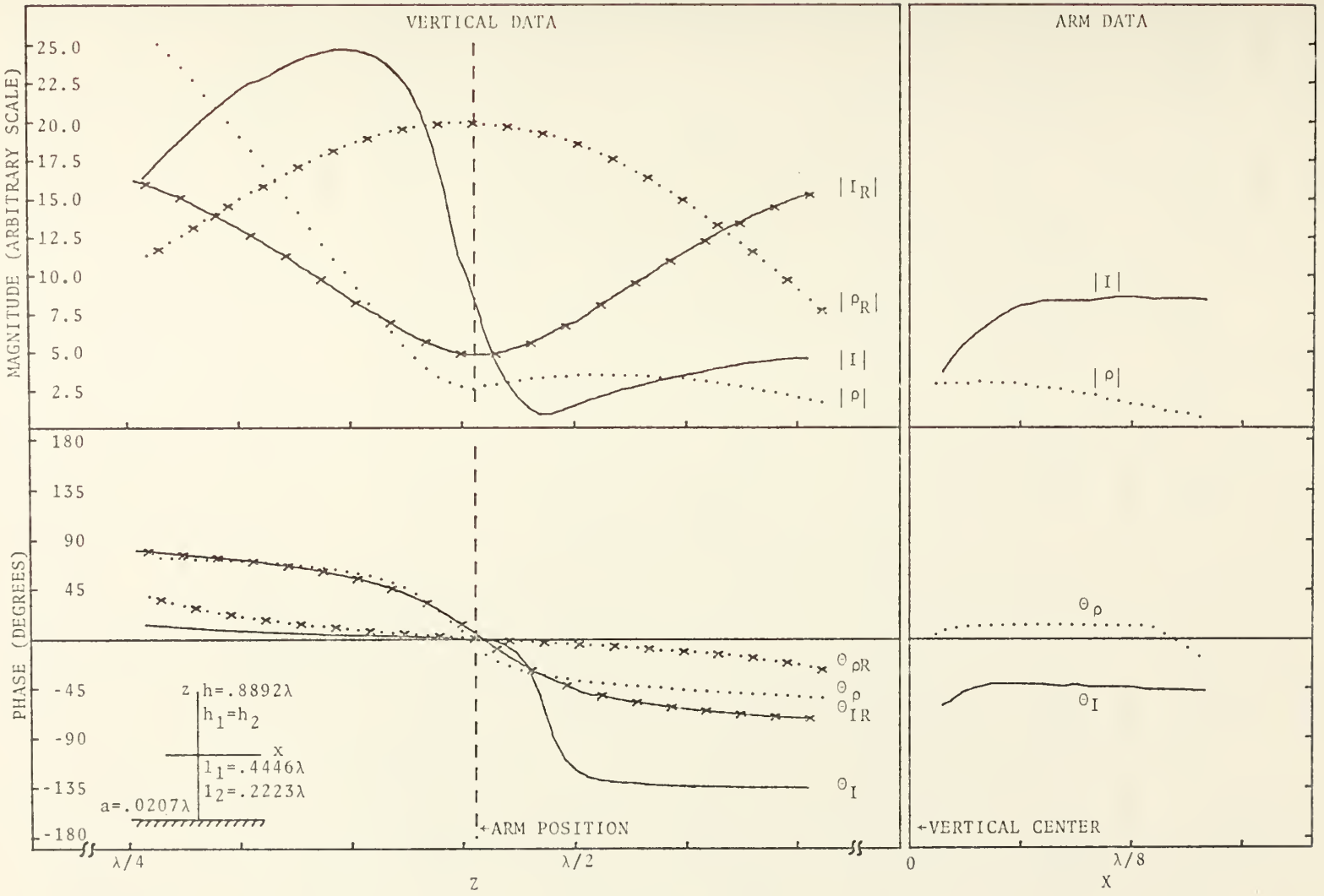

Figure 35. - Measured charges and currents on a transmitting monopole and crossed-monopole. Junction at maximum charge minimum current.

For this asymmetric case measurement of the current and charge from the axillary slot (see section III.C.2.) was also attempted. The results from this attempt were unsatisfactory; however, they are presented in Figures 36 and 37 and briefly discussed as an indication of the problems surrounding charge and current distribution measurement with this technique when the probes cannot be properly oriented with respect to each field component.

In Figures 36 and 37 the surface slot data for the CASE 5 configuration has been plotted as the reference, with every third data point indicated by an "X" and a subscript "R" added to the curve labels. In all cases the charge distribution plots from the surface slots and the axillary slots are in reasonably good agreement. The current distribution plots; however, are severely distorted. This distortion is believed to result from the interaction of the H fields from the vertical and horizontal elements within the current probe. When in the axillary slot the plane of the current probe is oriented perpendicular to the H fields of both the vertical and horizontal elements and therefore responds to both field components. As the vertical element is approached along the horizontal arm or vice versa the distortion of current magnitude becomes more severe supporting this theory. The solution of this problem and

measurement of charge and current distributions of other surface areas of the crossed-monopole is left for another thesis.

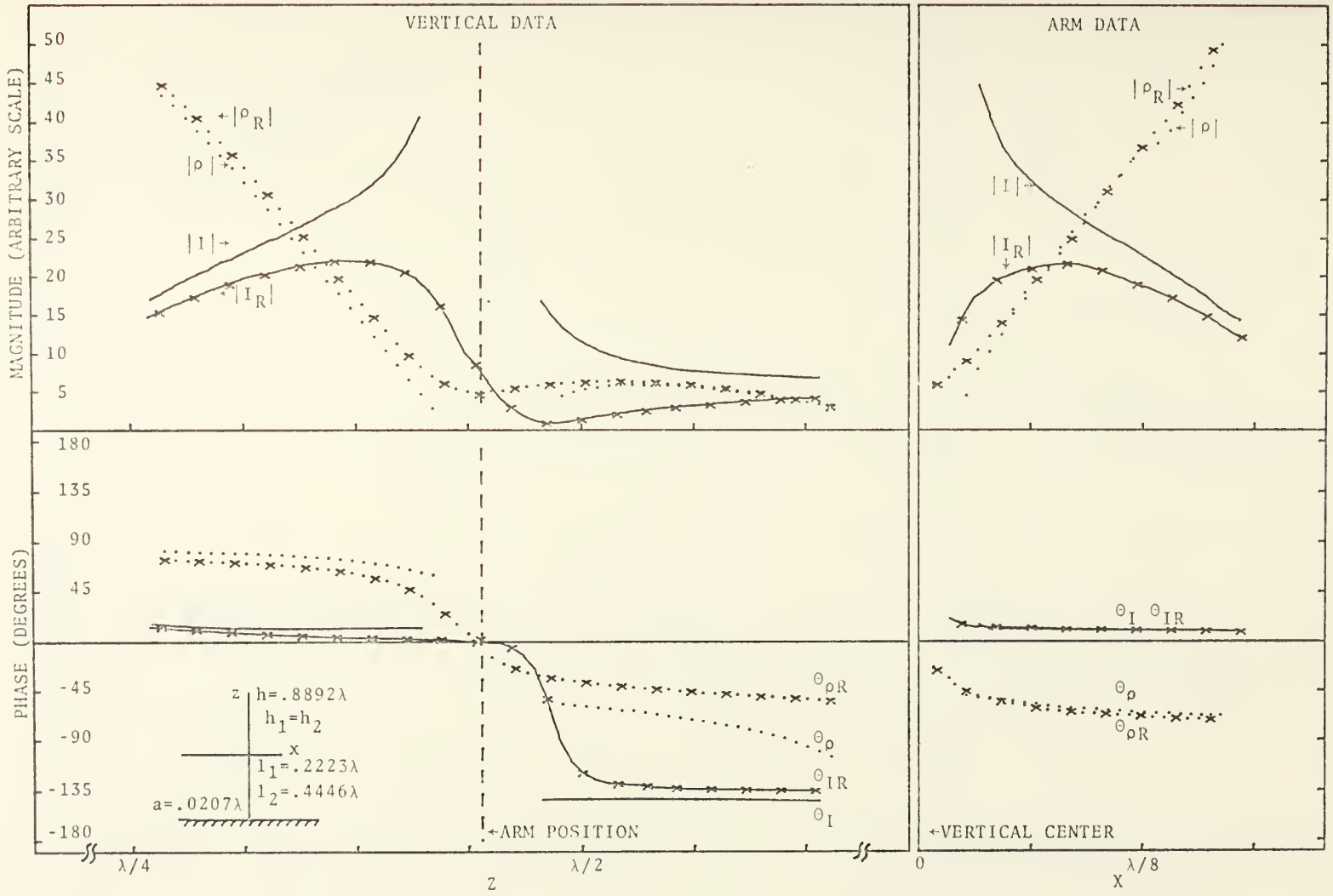

Figure 36. - Measured charge and current on a transmitting crossed-monopole. Comparing axillary and surface slot measurements.

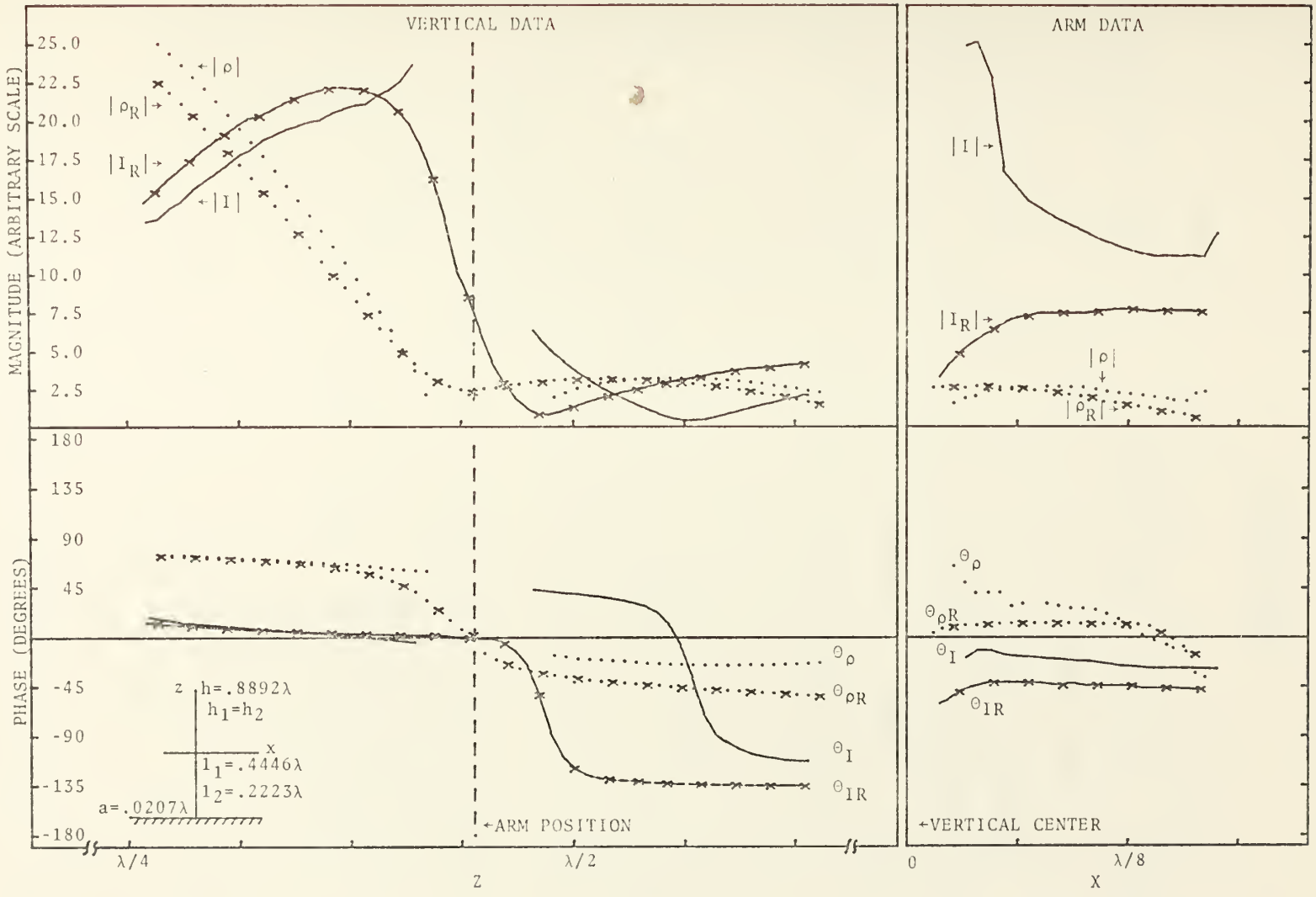

Figure 37. - Measured charge and current on a transmitting crossed-monopole. Comparing axillary and surface slot measurements.

VI. CONCLUSIONS

The addition of resonant and antiresonant length horizontal arms to a transmitting vertical monopole at either a point of maximum current/minimum charge or maximum charge/minimum current on the vertical monopole causes significant changes to the impedance and the charge and current distributions of the monopole. These changes are less pronounced when horizontal arms are placed at a point of charge minimum on the transmitting vertical monopole than when placed at a point of charge maximum. Under these conditions the resonant arm is capable of dominating the antenna and changing an otherwise antiresonant structure to a resonant structure.

The general form of the charge and current distributions on the resonant or antiresonant horizontal arms and on the portion of the vertical element above the junction can be predicted by considering the horizontal arms excited by the junction charge and the vertical extension above the junction excited by both the junction charge and the self inductance of the vertical element at the junction. An antiresonant length element excited by charge at the junction has a response which is purely antiresonant while a

resonant length element excited in the same manner has a charge and current standing-wave distribution which is the sum of the resonant and antiresonant responses of the element. On the other hand, excitation of a resonant length vertical extension above the junction through the self inductance of the vertical member results in a charge and current standing-wave pattern which is the resonant response while the same excitation of an antiresonant length upper vertical element results in a complex standing-wave distribution of charge and current which is the sum of the antiresonant and resonant responses of the element. By considering the sum of the appropriate responses described above with continuity of charge and Kirchoff's Current Law applied at the junction the appearance of the charge and current distributions on a crossed-monopole antenna composed of resonant and antiresonant length elements and the effect on input impedance of the addition of resonant or antiresonant horizontal arms to a monopole can be approximated.

BIBLIOGRAPHY

Brown, R. G., Sharpe, R. A., Hughes, W. L., and Post, R. E., Lines, Waves, and Antennas, The Transmission of Electric Energy, The Ronald Press Company, New York, 1973.

Burton, R. W., "The Crossed-Dipole Structure of Aircraft in an Electromagnetic Pulse Environment," Proceedings of The Conference on Electromagnetic Noise, Interference and Compatibility Advisory Group for Aerospace Research and Development (AGARD) NATO, p. 30-1 thru 30-15, Paris, France, October 1974.

Burton, R. W. and King, R. W. P., "Measured Currents and Charges on Thin Crossed Antennas in a Plane-Wave Field," IEEE Transactions on Antennas and Propagation, v. AP-23, No. 5, p. 657 - 664, September 1975.

Butler, C. M., "Currents Induced on a Pair of Skew Crossed Wires," IEEE Transactions on Antennas and Propagation, v. AP-20, p. 731 - 736, November 1972.

Chao, H. H. and Strait, B. J., "Radiation and Scattering by Configurations of Bent Wires with Junctions," IEEE Transactions on Antennas and Propagation, v. AP-19, p. 701 - 702, September 1972.

King, D. D., "Measured Impedance of Cylindrical Dipoles," Journal of Applied Physics, v. 17, p. 844, 1946.

King, R. W. P., The Theory of Linear Antennas, Harvard University Press, Cambridge, massachusetts, 1956.

King, R. W. P. and Wu, T. T., "Analysis of Crossed Wires in a Plane-Wave Field," IEEE Transactions on Electromagnetic Compatibility, v. EMC-17, p. 255 - 265, November 1975.

Spencer, R. C., Resonance of Electromagnetic Waves on Cross-Monopole Wire Structures, M.S.E.E. Thesis, Naval Postgraduate School, Monterey, California, June 1975.

Taylor, C. D., "Electromagnetic Scattering from Arbitrary Configurations of Wires," IEEE Transactions on Antennas and Propagation, v. AP-17, p. 662 - 663, 1969.

Taylor, C. D., Lin, S. M., and McAdams H. V., "Electromagnetic Scattering from Crossed Wires," IEEE Transactions on Antennas and Propagation, v. AP-18, p. 133 - 136, January 1970.

INITIAL DISTRIBUTION LIST

		No. Copies
1.	Defense Documentation Center Cameron Station Alexandria, Virginia 22314	2
2.	Library, Code 0212 Naval Postgraduate School Monterey, California 93940	2
3.	Department Chairman, Code 52 Department of Electrical Engineering Naval Postgraduate School Monterey, California 93940	2
4.	Assoc. Prof. Robert W. Burton, LTCOL, USAF Code 52Zn Department of Electrical Engineering Naval Postgraduate School Monterey, California 93940	15
5.	Elmer J. McDowell, LCDR, USN COMSECONDFLT Staff FPO New York 09501	3
6.	Post-Doctoral Program RADC-RBC Rome Air Development Center Griffiss AFB New York 13441	1

7. Mr. Philip Blacksmith 1
Code LZR
Air Force Research Lab.
Laurence G. Hanscom Field
Bedford, Massachusetts 01730

8. Air Force Weapons Laboratory/PRP 2
Kirtland AFB
New Mexico 87117